Revision 1

Experimental and infrared characterization of the miscibility gap along the tremolite-glaucophane join

by

David M. Jenkins[1], Michael A. Carpenter[2], and Ming Zhang[2]

[1]Department of Geological Sciences and Environmental Studies, Binghamton University, Binghamton, NY, 13902-6000, U.S.A.

[2] Department of Earth Sciences, University of Cambridge, Cambridge CB2 3EQ, UK

Abstract

Knowledge of the thermodynamic mixing properties of amphiboles whose compositions lie along the tremolite-glaucophane join is of interest to those studying high-pressure metamorphic rocks as well as rocks transitional between the greenschist and blueschist facies. This study is the second of a two-part investigation of the tremolite-glaucophane join, with the first study (Jenkins et al., 2013, Amer. Mineral., 98, 588-600) devoted to the volume-composition and crystal-chemical relations, and the current study focused on defining the location and extent of asymmetry of the miscibility gap (solvus) along this join. A series of experiments was done over the temperature range of 500 – 800°C at pressures of 1.6-1.9 GPa to determine the location of the miscibility gap using both two-amphibole dissolution experiments, including time-series experiments at 700, 750, and 800°C lasting up to 670 h, as well as a variety of end-member and intermediate amphibole overgrowth techniques to approach the boundary from different compositional directions. These results, which placed some important limits on the location of the miscibility gap, were combined with an autocorrelation analysis of the mid- and far-infrared

spectra of single-phase amphiboles formed in the first study (Jenkins, 2013) to refine the shape of the miscibility gap. Derived values of the relative change in the autocorrelation parameter ($\delta\Delta$Corr) were fairly constant over all of the frequency ranges analyzed and indicated that the miscibility gap is steeper at the glaucophane-rich compared to tremolite-rich side of the binary join. Combining the compositional re-equilibration experiments with the infrared autocorrelation results permitted deriving the ratio of the parameters $\alpha_{Gl}/\alpha_{Tr} = 0.5$ and $W_{TrGl} = 67$-70 kJ using asymmetric formalism theory. The calculated boundary has a critical-point temperature that falls in the range of 760-800° C in this iron-free system. The asymmetry of the calculated miscibility gap appears to be confirmed by amphibole pairs in Nature. The implications of this study are that this technique of combining compositional re-equilibration experiments with autocorrelation analysis of single-phase solid solutions is a potentially powerful method of locating miscibility gaps at low temperatures and for chemically complex binary joins. It is also suggested that the miscibility gaps presented here provide a basis for interpreting the degree of equilibrium reached in assemblages with complexly zoned or intergrown amphiboles.

Keywords: glaucophane, tremolite, miscibility gap, autocorrelation analysis, FTIR

Introduction

Amphiboles along the join tremolite, $\square Ca_2Mg_5Si_8O_{22}(OH)_2$ (= Tr, where $\square$ represents a vacancy), and glaucophane, $\square Na_2Mg_3Al_2Si_8O_{22}(OH)_2$ (= Gl), are of interest because they model the complete spectrum of compositional variations from lower-pressure greenschist to higher-pressure blueschist facies rocks in the iron-free system Na_2O-CaO-MgO-Al_2O_3-SiO_2-H_2O

(NCMASH). Understanding the thermodynamic mixing properties along this join will serve as an important framework for deducing the conditions of metamorphism from more chemically complex and Fe-bearing amphiboles.

One important aspect that must be considered for this join is the likely presence of a miscibility gap. There have been a number of detailed studies of metamorphic rocks (e.g., Himmelberg and Papike, 1969; Maresch et al., 1982; Liou and Maruyama, 1987; Reynard and Ballèvre, 1988; Smelik and Veblen, 1992) reporting that glaucophane shares a miscibility gap, rather than complete solid solution, with calcic amphiboles. Aside from the importance of knowing the location of a miscibility gap in pressure-temperature (*P*-*T*) space for the purpose of interpreting the metamorphic conditions from amphibole compositions, it can be very useful for the thermochemical study of a mineral join. In the thermodynamic modeling of Ca- and Na-bearing clinoamphiboles presented by Dale et al. (2005), it was stressed that the size and shape of solvi are very sensitive to the excess enthalpy of mixing which, in turn, can provide an excellent means of calibrating the thermodynamic activity models.

This study is the second of a two-part investigation of the tremolite-glaucophane join, the first being a report of the crystal-chemical properties by Jenkins et al. (2013). Here we report experimental results aimed at defining the location of the miscibility gap in temperature-composition space. In particular, compositional re-equilibration experiments are reported which can be used to define the maximum and minimum width of the miscibility gap in separate experiments (i.e., separate half brackets) using different types of starting materials in the NCMASH system. In addition, results of the autocorrelation analysis (e.g., Salje et al., 2000; Boffa Ballaran and Carpenter, 2003) of infrared spectra of amphiboles formed at 10 mol%

69 increments along the tremolite-glaucophane join are presented and are used to show that the
70 shape of the miscibility gap can be independently determined.

71 ## Methods

72 ### Starting materials and experimental apparatus

73 A detailed description of the synthesis and characterization of the amphiboles used in this study
74 is given in Jenkins et al. (2013). Additional phases were synthesized as follows. All phases
75 were made from reagent-grade oxides and carbonates or hydroxides formed from these materials.
76 In particular, the source of SiO_2 was desiccated silicic acid, heated in steps to a maximum
77 temperature of 1100°C and yielding amorphous silica or weakly crystalline cristobalite. The
78 source of aluminum was Al_2O_3, sodium was Na_2CO_3, calcium was either $CaCO_3$ or $Ca(OH)_2$,
79 and magnesium was either MgO or $Mg(OH)_2$. The hydroxides $Ca(OH)_2$ and $Mg(OH)_2$, which
80 are a convenient way to introduce controlled amounts of water and were observed in some cases
81 to give higher synthesis yields of amphibole, were made by roasting $CaCO_3$ and MgO,
82 respectively, at 1100°C for several hours and then heating the resultant oxides with water until
83 dry. The purity of the hydroxides was checked by X-ray diffraction, indicating essentially pure
84 $Ca(OH)_2$ was obtained and that nearly pure $Mg(OH)_2$ was obtained with only very minor (0.6
85 wt%) unreacted MgO present. Starting mixtures that were prepared with carbonates were
86 decarbonated by heating in air at 900°C for 15 minutes, which was sufficient to remove CO_2 by
87 reaction with silica. Any hydroxides used were added after decarbonation. The bulk
88 compositions of phases and oxide/hydroxide mixtures used in this study are listed in Table 1.

89 Experiments below 0.5 GPa were done in internally-heated gas vessels using Ar as the
90 pressure medium with two Inconel®-sheathed chromel-alumel thermocouples situated across the
91 length of the capsule to monitor the temperature as well as the thermal gradient across the

capsule length. Experiments in the range of 1.5-2.5 GPa were done in a ½-inch diameter piston-cylinder press using NaCl as the pressure medium and a straight graphite furnace. Temperatures were monitored and controlled with a chromel-alumel thermocouple positioned directly above the sample. Syntheses were done by sealing portions of the starting mixtures along with specific weight percentages of distilled water, or simply as a dry mixture if excess water was present in a hydroxide reagent, in 5 mm outer diameter (OD) Pt capsules that were 18 mm long with wall thicknesses of 0.13-0.18 mm. The specific conditions used for synthesizing the starting materials and weight percentages of water used in the syntheses are listed in Table 1. Mixtures of synthetic phases, i.e., re-equilibration mixtures, were treated in 1.5 mm OD Pt capsules of 8 mm length with the same wall thicknesses. The phases used in these re-equilibration mixtures are given in Table 2 and the conditions of treatment are listed in Table 3.

Analytical equipment and methods

Powder X-ray diffraction analysis and Rietveld refinements were done at Binghamton University using a Philips Xpert PW3040-MPD diffractometer operated at 40 kV and 20 mA using Cu-Kα radiation and fitted with a diffracted-beam graphite monochromator. Samples used in the re-equilibration experiments were limited in quantity (~5 mg) and, when mounted on zero-background oriented quartz plates as thin smears, occupied areas considerably smaller than the X-ray beam at low angles and yielded very low counts at high angles. Routine phase identification was done one samples scanned from 8 – 50° 2θ with step sizes of 0.02° 2θ for durations sufficient to obtain about 1000 counts on the strongest reflections. Because the primary goal of the Rietveld refinements was to obtain unit-cell dimensions, the refinements were made using the range of 12 to 50° 2θ where the strongest reflections occur and where the X-ray beam is essentially fully on the sample area. This angular range, though certainly not

optimal for full structure refinement, is sufficient for unit-cell dimensions for amphiboles and includes about 80 reflections. Rietveld refinements were done using the program GSAS (Larson and Von Dreele, 2000) and initiating the refinements by using the structures of tremolite from Hawthorne and Grundy (1976), winchite from Sokolova et al. (2001), glaucophane from Papike and Clark (1968), quartz from Levien et al. (1980), talc from Perdikatsis and Burzlaff (1981), omphacite (*P*2/*n*) from Pavese et al. (2000), enstatite from Nestola et al. (2006), and clino-enstatite from Ohashi (1984). Quartz (a_0 = 4.91390, c_0 = 5.40595 Å) is present in most of the samples at ~5 wt% and provides an internal standard against which the zeropoint could be refined, typically with a precision of 0.005-0.008° 2θ. Reagent NaCl (a_0 = 5.6401 Å) was added as an internal standard to the few samples without quartz. Refined parameters included the background (Function 1, shifted Chebyshev), zeropoint, profile parameters (LX and LY, with asym = 0.0), March-Dollase preferred orientation, and cell dimensions of the major phases. Typical whole-pattern agreement indices were R_P of 8-15%, R_{WP} of 11-22%, χ^2 of 1.5-4 (or goodness-of-fit of 1.2 – 2), and Durbin-Watson *d* statistics of 0.7 – 1.4. In view of these somewhat low values for the Durbin-Watson *d* statistic, the uncertainties for the unit-cell dimensions may be underestimated by up to 50% (Hill and Flack, 1987).

Electron microprobe (EMP) analysis was done on a JEOL 8900 Superprobe using samples mounted in epoxy and polished in steps to a final 0.5 μm diamond grit size. Operating conditions for all analyses were 15 kV and 10 nA using albite as the standard for Na, diopside for Ca, and the pure oxides for Mg, Al, and Si. Matrix corrections were made with the ZAF scheme. Sodium X-ray counts were monitored for the glaucophane-rich amphiboles made in this study to check for the extent of Na diffusion under the electron beam, but none was observed for counting durations of 1 minute in spot mode (~ 1 μm diameter). Even so, the counting times for

WDS analyses were kept to 10 s on the peak and 3 s on the background to minimize Na diffusion from either the albite standard or the sample.

Powder infrared spectra in the mid-infrared (MIR) range of 350-5000 cm^{-1} were obtained at the University of Cambridge using a Bruker IFS 66v evacuable infrared spectrometer fitted with a deuterated triglycine sulfate (DTGS) detector, KBr window, KBr beamsplitter, and a globar lamp source. Samples were prepared as compressed KBr pellets using a sample:KBr ratio of 1:300 and a total pellet mass of 200 mg. Spectra were collected with 512 scans at 2 cm^{-1} resolution. Spectra in the far-infrared (FIR) range of 50-1900 cm^{-1} were measured with a Bruker IFS 113v evacuable spectrometer fitted with a DTGS detector, polyethylene window, mylar beamsplitter, and mercury lamp source. Spectra were collected with 500 scans at a resolution of 2 cm^{-1}. Samples were prepared as compressed polyethylene pellets using a sample:polyethylene ratio of 1:50 and a total pellet mass of 100 mg. All spectra were measured in absorption mode.

Results

Tremolite and glaucophane re-equilibration

Synthetic tremolite (TREM 23-13) and glaucophane (FEGL 5-2-7), whose compositions are given in Table 4, were combined in equi-molar proportions to give the bulk composition $Tr_{45}Mc_5Gl_{50}$, where Mc = $Mg_7Si_8O_{22}(OH)_2$, shown as point 2 in Figure 1a. This mixture was treated at the conditions listed in Table 3 for the GLTR 2-series experiments. These experiments, involving the compositional re-equilibration of the two end members, will most likely define the maximum width of the miscibility gap along this join with the true width being reached only in the absence of any kinetic barriers. Electron microprobe analysis was initially used to monitor the extent of compositional re-equilibration. Figures 2a-d show all accepted analyses of individual amphiboles (open circles) from experiments done at 500-800°C using a

projection from $Mg_7Si_8O_{22}(OH)_2$ and H_2O onto the ternary diagram ($NaO_{0.5}$+$AlO_{1.5}$)-CaO-SiO_2, which permits variations in the SiO_2 content of the amphibole to be shown. Unfortunately convergence of the analyses to a well-defined limit of amphibole composition was not observed in most cases, with the results at 600°C (Fig. 2b) showing possible clusterings defining a miscibility gap. The reason for this lack of convergence is unknown but is attributed primarily to the fine grain sizes of the synthetic tremolite and glaucophane dealt with here, making it much harder to discern core-to-rim compositional re-equilibrations as was observed, for example, for the aluminous tremolites investigated by Jenkins (1994). The lack of shift in analyses at 500°C away from the SiO_2 apex, as seen at higher temperatures, suggests that the spread in analyses arises more from overlapping fine grains than from re-equilibrated compositions.

An alternative approach is to use the unit-cell volumes of the coexisting amphiboles as a means of determining the aggregate composition of an entire population of amphibole grains. Figure 3 compares portions of the powder XRD patterns of the GLTR-2 starting mixture (Mix, Table 2) at the bottom with those after treatment at 600° (GLTR 2-2, Table 3), 700° (GLTR 2-3, Table 3), and 800°C (GLTR 2-4, Table 3). In addition to some subtle changes in peak position, made more apparent when compared to the vertical lines for the 240 and 310 peaks, there are also obvious loss or merging of peaks as the sample homogenizes to a single amphibole at the highest temperature. Quartz, used as an internal standard, is readily seen in these patterns. The unit-cell volumes of the amphiboles synethesized along the tremolite-glaucophane join by Jenkins et al. (2013) were derived by Rietveld refinement in the same manner as was used in this study, yielding the following polynomial expression for the volume-composition relationships:

$$V(\text{Å}^3) = 865.3 \pm 0.5 + (77.6 \pm 5.6)^B X_{\text{Ca}} - (37.6 \pm 6.6)(^B X_{\text{Ca}})^2 \quad (1)$$

where volume (V) is expressed as a function of the mole fraction of B-site (M4) Ca. The uncertainties given in equation (1) are dominated by the large uncertainties (5-15% relative standard deviation, rsd, for Ca-rich samples) in the compositions of the amphiboles determined by electron microprobe analysis, compared to the small uncertainties in the volumes (0.01-0.05% rsd), determined by Rietveld refinement. One can use equation (1) to determine the value of ${}^{B}X_{\mathrm{Ca}}$ that corresponds to an observed volume. Calcium contents based on equation (1), but reported as atoms per formula unit (apfu = $2\cdot {}^{B}X_{\mathrm{Ca}}$), for all of the amphibole re-equilibration experiments are reported in Table 5. It is important to note that the volume-composition relationships derived for this join apply even if the amphiboles near the middle of the tremolite-glaucophane join are shifted substantially (up to 39 mol%) toward katophorite ($(\mathrm{Na(NaCa)(Mg_4Al)(AlSi_7)O_{22}(OH)_2})$).

The compositions of the GLTR-2-series re-equilibration experiments are shown by the solid circles on the temperature-composition diagram in Figure 4. The starting amphibole compositions are shown as vertical dashed lines.

Demonstrating that equilibrium has been reached during the re-equilibration of amphibole end-member compositions is challenging. Ultimately there will be a temperature below which the kinetics of the process become prohibitively slow on an experimental timeframe. Figure 5 shows the results of a series of experiments done at 700, 750, and 800° C. At 700°C two amphiboles are still present after 670, whereas at 750 and 800°C the two amphiboles have merged into one Tr-enriched amphibole. These latter two results provide an important upper-temperature limit on the location of the miscibility gap for the GLTR-2 bulk composition corresponding to 0.9 Ca apfu. The amphibole compositions of these time-series experiments are also shown as solid circles in Figure 4, with the arrows indicating the sense of compositional

change from the starting amphibole compositions. The right-pointing arrows at 750° and 800°C emphasize that the two amphiboles merged to a single composition at these temperatures. It is stressed that this experimental approach can only define the maximum width of the miscibility gap, as sluggish kinetics at ever lower temperatures may eventually prohibit convergence to the equilibrium boundary.

Amphibole-omphacite-talc experiments

Two sets of experiments were done to try and define the maximum width of the miscibility gap using a slightly different approach. One starting mixture consisted of tremolite, omphacite, and talc with a bulk composition of $Tr_{54}Mc_6Gl_{40}$ (GLTR-3-series), while a second consisted of glaucophane, omphacite, and talc with a bulk composition of $Tr_{36}Mc_4Gl_{60}$ (GLTR-4-series). The bulk compositions of these mixtures are indicated as points 3 and 4 in Figure 1b. These experiments were designed to induce compositional changes in the seed amphibole by reaction of omphacite and talc, which may prove more reactive than the direct equilibration of previously synthesized amphiboles. Results are listed in Table 3, and the compositions of the amphiboles, as determined from their unit-cell volumes, are listed in Table 5 and plotted as the open circles in Figure 4. Several things should be noted about these experiments. In general there was a single amphibole after treatment, usually shifted from the initial composition (vertical lines, Fig. 4), except for GLTR 4-2 at 700°C, which spontaneously nucleated a Tr-rich amphibole while maintaining a Gl-rich seed amphibole. This is taken as a strong indication that this experiment at 700°C is below the critical point. Second, both experiments at 800°C produced single-phase Tr-rich amphiboles even though they started with very different seed-amphibole compositions, suggesting conditions that are above the critical point. The compositions of the 800°C amphiboles are both shifted noticeably toward Ca enrichment relative to the bulk compositions

of the starting mixtures; mass balance for these experiments are, however, maintained by the presence of Ca-poor pyroxenes. Overall there is broad agreement in the maximum extent of the miscibility gap between the two-amphibole re-equilibration experiments described above and the amphibole-omphacite-talc experiments.

Winchitic amphibole seed experiments

Two sets of experiments were done in an attempt to approach the boundary from inside the miscibility gap. In these experiments an intermediate amphibole approximately of winchite composition [WIN 11-3, $(Na_{1.2}Ca_{0.8})(Mg_{3.8}Al_{1.2})Si_8O_{22}(OH)_2$] was treated either in the presence of a tremolite-oxide mixture with the bulk composition of $Tr_{50}Mc_1Gl_{49}$ (GLTR-5) or in the presence of a glaucophane-oxide mixture with the bulk composition of $Tr_{30}Gl_{70}$ (GLTR-6). The GLTR-5-series of experiments (bulk composition 5 in Figure 1c) formed amphiboles whose compositions all converged to that of the seed amphibole, as confirmed by both electron microprobe analysis and the volume-composition relations (Table 5). This occurred at all temperatures investigated, namely over the range of 500-750°C in 50° increments. The reason why there is only a single amphibole is not known. Two possible explanations are that the reactivity of the tremolite oxide mixture with winchite was sufficiently rapid that it simply formed additional amphibole of the same bulk composition at all temperatures, or that the formation of a separate tremolite-rich amphibole was prevented because the bulk composition lies too close to the spinodal boundary (e.g., Spear, 1995, p. 200). The GLTR-6-series of experiments (point 6 in Figure 1c) was different, in that a two-amphibole assemblage was detected at each temperature investigated. Inspection by back-scattered electron imaging of samples treated at temperatures below 750°C usually did not reveal any obvious overgrowths on the winchite seeds; however, overgrowths were discernible for the sample treated at 750°C, as

252 shown in Figure 6 and confirmed by direct analysis of the cores and rims of the grains in this
253 image. The presence of overgrowths in this sample is presumably caused by the enhanced
254 kinetics and greater degree of rim growth at this higher temperature. The glaucophane-rich
255 amphibole that formed shows a slight but systematic enrichment in Ca with increasing
256 temperature, as seen by the open squares in Figure 4. As with the GLTR-5-series experiments,
257 these glaucophane-rich amphiboles may lie along the spinodal boundary and, therefore, would
258 surely represent a maximum Ca content for the equilibrium (binodal) gap.

259 Based on all of the re-equilibration results in Figure 4 it is apparent that the miscibility gap is
260 asymmetric, with the Ca-rich side having greater solid solution than the Ca-poor side. This is
261 consistent with other miscibility gaps where the small-volume phase tends to have more
262 restricted solid solution than the large-volume phase, as seen, for example, for the calcite-
263 dolomite (Goldsmith and Heard, 1961) or alkali feldspar (Hovis et al., 1991) joins. It is also
264 consistent with the compositions of coexisting amphiboles in Nature, as discussed below.

265 **Autocorrelation analysis**

266 The spectrum-analysis method known as autocorrelation, as applied to infrared spectra, has been
267 advocated by a number of researchers as a way of using strain-induced broadening of vibrational
268 spectra to extract information for such things as phase transitions, cation mixing in solid
269 solutions, and atomic order-disorder (e.g., Salje et al. 2000, Tarantino et al. 2002, Boffa Ballaran
270 and Carpenter 2003, Etzel and Benisek 2008, Koch-Müller et al. 2012). In brief, autocorrelation
271 is a way of extracting the amount of band broadening in spectra that are asymmetric and often
272 consisting of overlapping bands. The autocorrelation function, which correlates a spectrum
273 against itself but offset in successive increments of frequency over the frequency range of
274 interest, can provide a symmetric rendering of complex infrared spectra from which the band

width is more systematically determined. The parameter of interest, Δ*Corr*, is the width of the autocorrelated spectrum at the limit of zero frequency shift. It is this parameter, or more generally the difference in Δ*Corr* for a particular intermediate solid-solution relative to a mechanical mixture of the end-members (i.e., δΔ*Corr*), that can be related to the amount of strain energy and enthalpy of mixing (e.g., Boffa Ballaran and Carpenter 2003, Etzel and Benisek 2008). A detailed discussion and worked examples of the autocorrelation method can be found in Salje et al. (2000). In this study it is used as an independent method of verifying the positive enthalpy of mixing and, perhaps more importantly, for deriving the degree of asymmetry of the miscibility gap along the tremolite-glaucophane join.

Infrared spectra were obtained for amphiboles synthesized from mixtures prepared at 10 mol% increments along the tremolite-glaucophane join. They were synthesized at conditions above the miscibility gap ranging from 840°C and 0.6 GPa to 750°C and 2.5 GPa for Tr- and Gl-rich amphiboles, respectively. These samples were described in detail in Jenkins et al. (2013) and are summarized here in Table 6 which lists their sample codes, nominal and observed Ca contents (via electron microprobe), unit-cell volumes measured in this study, and Ca contents derived from equation (1), the latter providing a basis for comparison with the amphibole compositions shown in Figures 4 and 5.

The mid- and far-infrared spectra are shown in Figures 7a and 7b, respectively. One can see the distinct broadening of the spectra starting from tremolite (bottom spectrum) and reaching a maximum in the range of 60-80 mol% Gl. This broadening is consistent with the development of increasing strain energy as a phase experiences increasing solid solution (e.g., Carpenter et al., 1999). The spectrum of end-member glaucophane (top) is somewhat broader than that of

297 tremolite, which may be caused by the additional cation mixing of Mg and Al on the octahedral
298 sites.

299 Autocorrelation analysis does not require that the origin of the vibrations (i.e., band
300 assignments) be known; however, mapping the changes in band positions across the solid
301 solution series can help distinguish band broadening arising from the merging of separate bands
302 as compared to the development of strain in the lattice. The spectra were modeled using
303 symmetric pseudo-Voigt (50% Gaussian) peaks with similar widths; the resulting peak positions
304 are shown in Figures 8a and 8b as a function of sample composition. In general, the mid-
305 infrared spectra consist of bands that can be traced across the compositional join with an overall
306 shift toward decreasing frequencies with increasing Tr content. The far-infrared spectra show
307 the loss (bands 23 and 34) and appearance (24') of some bands, but in general the spectra consist
308 of separable bands that vary continuously across the join and shift to lower frequencies with
309 increasing Tr content, as for the mid-infrared spectra.

310 Regions of the spectra to which linear backgrounds could be readily fitted were chosen for
311 autocorrelation analysis. In the mid-infrared range these were: 400-600 cm^{-1} (bands 1-7); 650-
312 700 cm^{-1} (bands 8-10); 720-800 cm^{-1} (bands 11-14); and 850-1200 cm^{-1} (bands 15-22). These
313 regions correspond in general to tetrahedral chain bending, O-Si-O chain deformation and OH-
314 librations, Si-O-Si deformations, and Si-O stretching, respectively (Andrut et al. 2000,
315 Hofmeister and Bowey 2006; Ishida et al. 2008). Regions used in the far-infrared were: 100-200
316 cm^{-1} (bands 23-26); and 200-275 cm^{-1} (bands 27-31). The former region has been associated
317 with translations of Mg or of the tetrahedral chain, while the latter has been associated with
318 translations of Ca or with Mg-O stretching (Hofmeister and Bowey 2006). The set of bands in

the range of 275-325 cm^{-1} (numbers 32-35, Fig. 8b) did not maintain a linear baseline and were therefore not used.

Figure 9 shows the autocorrelation results for the MIR (Figure 9a-d) and FIR (Figure 9e,f) ranges. In all cases it is clear that there is a positive deviation from the end-members, suggesting a positive enthalpy of mixing, though the sense of asymmetry is not always the same. The curves shown in these figures are simple polynomial fits to the data and have no theoretical basis. Figure 10 shows the same autocorrelation data as in Figure 9 but recast in terms $\delta\Delta Corr$ (cm^{-1}), which is the excess value of $\Delta Corr$ over that expected from a linear combination of the end-members and shown graphically by the double-headed arrows in Figure 9. It is the $\delta\Delta Corr$ values that have been correlated with the enthalpy of mixing (e.g., Boffa Ballaran and Carpenter 2003; Etzel and Benisek 2008). The curves shown in Figure 10 were fitted to the data using an equation analogous to the asymmetric formalism (ASF) treatment used by Holland and Powell (2003). In the ASF treatment, one can model the non-ideal mixing along a binary join of essentially any chemical complexity using three parameters: a macroscopic interaction parameter (W_{TrGl}) and two size parameters (α_{Tr} and α_{Gl}), one for each end member, whose relative values can be used to account for the asymmetry along the binary join. Because it is only the relative values of α_i that are important, it is customary to set one parameter to unity, which is normally the α_{Tr} parameter (Dale et al. 2005, Diener et al. 2007, Diener and Powell 2012). Adopting this convention, the excess Gibbs free energy of mixing (ΔG^{ex}), which, to a first approximation, is assumed to be equal to the enthalpy of mixing (ΔH^{mix}) and therefore proportional to $\delta\Delta Corr$, can be expressed as:

$$\Delta H^{mix} \propto \delta\Delta Corr = \left\{ \frac{X_{\mathrm{Tr}}(1-X_{\mathrm{Tr}})\alpha_{\mathrm{Gl}}}{\left[X_{\mathrm{Tr}}+(1-X)\alpha_{\mathrm{Gl}}\right]^2} \right\} \left\{ \frac{2\left[X_{\mathrm{Tr}}+(1-X_{\mathrm{Tr}})\alpha_{\mathrm{Gl}}\right]}{(1+\alpha_{\mathrm{Gl}})} \right\} W_{\mathrm{Corr}} \qquad (2)$$

where X_{Tr} is the mole fraction of Tr and is taken as the mole fraction of Ca in the M(4) site. The least-squares regression values of W_{Corr} and α_{Gl} for each frequency range are indicated on Figure 10. The derived values of W_{Corr} shown in Figure 10 are controlled by the absolute IR band intensity and specific frequency range over which the autocorrelation is done and, as such, have no physical meaning. The values of α_{Gl}, however, are a direct indication of the asymmetry of the $\delta\Delta Corr$ curve and presumably of the enthalpy of mixing. One can see that the values of α_{Gl} range from 0.24 to 1.02, with the average of all ranges being 0.58 ± 0.26 (1σ). Having a derived size parameter for α_{Gl} less than 1.0 is consistent with glaucophane being the smaller volume end member (Table 6).

Discussion

The primary goal of this study is to use the compositional re-equilibration and autocorrelation data to place limits on the location and shape, respectively, of the miscibility gap (i.e., solvus) along the tremolite-glaucophane join. As noted by Dale et al. (2005), the size and shape of amphibole miscibility gaps are very sensitive to the thermochemical parameters describing the mixing of amphibole components along a binary join.

The amphibole re-equilibration data provide two limits on the location of the miscibility gap. First, the re-equilibration experiments involving the mutual solution of the two end members, namely the solid circles in Figure 4, the time-series data in Figure 5, and the reaction of end-member amphiboles with omphacite and talc shown as the open circles in Figure 4, should define the maximum width of the miscibility gap. Second, the reaction of winchitic amphibole seeds with oxide/hydroxide mixtures of end-member amphibole compositions is proposed as one way of approaching the boundary from the other direction (inside the gap) as compared to the prohibitively slow process of unmixing single-phase amphiboles. This method appears to have

364 worked only for the glaucophane-mix—winchite assemblage (GLTR-6-series experiments, Table
365 5), whereby the amphibole overgrowths, shown as the open squares in Figure 4, are
366 compositionally distinct from the winchite seeds and from the bulk composition of the mixture.
367 The highest-temperature point in this series (GLTR 6-6), whether it is part of the chemical solvus
368 or spinode, provides a minimum temperature for the critical point of the miscibility gap.

369 The variable asymmetry in the $\delta\Delta Corr$ curves shown in Figure 10 requires us to make some
370 choice as to which value is deemed accurate. Because the length scale of a given phonon
371 vibration should increase with wavelength (or decreasing wavenumber) (e.g., Carpenter et al.,
372 1999), it is reasonable to propose that the far-infrared, rather than the near- or mid-infrared,
373 range would provide information on strain heterogeneities over distances of several unit cells
374 (Boffa Ballaran and Carpenter, 2003). Empirical observations from some studies have supported
375 this, whereby the lower frequencies have shown the clearest correlation with the enthalpy of
376 mixing (e.g., Tarantino et al. 2002; 2003, Boffa Ballaran and Carpenter 2003). In this case an α_{Gl}
377 of 0.51 ± 0.11 based on the $\delta\Delta Corr_{100}$ results would be the preferred value. In contrast, Etzel and
378 Benisek (2008) found the tetrahedral cation (T-O) stretching bands in the MIR range of 700-
379 1300 cm^{-1} to provide results that are more consistent with the known enthalpy of mixing of other
380 mineral joins when plotting the ΔH^{mix} versus $\delta\Delta Corr$ slope values against the integrated excess
381 volume of mixing, all normalized to one atom per formula unit (also see below). Similarly, a
382 preliminary study of the autocorrelation results of synthetic carbonates along the calcite-dolomite
383 join by Holmes et al. (2012) showed that only the strong CO_3 stretching/bending vibrations in the
384 MIR range (700-1400 cm^{-1}) yielded $\delta\Delta Corr$ values with the same negative deviations in the 0 –
385 15 mol% $MgCO_3$ range as that observed by the solution calorimetry results of Navrotsky and
386 Capobianco (1987). This range would be analogous to the Si-O stretching vibrations at 850-

1200 cm^{-1} for the tremolite-glaucophane join studied here, which gave a nearly identical α_{Gl} value of 0.51 ± 0.02 as the lowest-frequency range. Such close agreement may be fortuitous, but α_{Gl} values around 0.51 are observed from other frequency ranges and suggest that similar strain energies are being sensed by phonon vibrations at a variety of length scales.

The autocorrelation results shown in Figures 9 and 10 are based on the assumption that all samples lie strictly on the tremolite-glaucophane join. As discussed by Jenkins et al. (2013), amphiboles synthesized from mixtures prepared near the middle of this join show a deviation from the expected composition that is most closely approximated by solid solution with up to as much as ~35 mol% katophorite ($Na(NaCa)(Mg_4Al)(AlSi_7)O_{22}(OH)_2$ = Kt), a component that combines the exchange vectors $NaAlSi_{-1}$ (edenite) and $NaAlCa_{-1}Mg_{-1}$ (0.5 glaucophane) with tremolite. Although the effect of this non-binary component is unknown in this study, it is considered not to be the dominant source of strain energy because the excess volume of mixing is essentially the same for the tremolite-glaucophane join after the observed volumes have been corrected for the Kt component. Nevertheless, an additional set of curves (dotted) were fitted to the $\delta\Delta Corr$ data in Figure 10 for only the two most Gl-rich and three most Tr-rich samples, that is only for the samples whose compositions lie closest to the tremolite-glaucophane join. The derived values of α_{Gl} are given in square brackets and, for all but two frequency ranges, are the same within error. The average value of α_{Gl} for all the frequency ranges is 0.6 ± 0.3, which is identical to that obtained when all of the data (i.e., solid curves) are used. Based on the similarity of results, using either the entire data set or only those samples closest to the tremolite-glaucophane join, it is concluded that the strain energy is dominated by the mixing of tremolite and glaucophane components.

Using an α_{Gl} of 0.51, one can determine a macroscopic interaction parameter (W_{TrGl}) that yields a calculated miscibility gap that fits the compositional re-equilibration data in Figure 4. Two such curves are shown in Figure 4. The solid curve is for a W_{TrGl} of 70 kJ and passes inside the Gl-rich dissolution (solid circle) and tremolite-omphacite-talc (open circle) data points. It is considered to be the highest-temperature boundary consistent with the data, having a calculated critical point at 805°C and 0.55 Ca (apfu). The dotted curve is for a W_{TrGl} of 67 kJ, and is constrained to pass through the winchite-overgrowth point at 750°C (open square). It is considered to be the lowest-temperature boundary consistent with these overgrowth experiments and has a calculated critical point at 762°C and 0.55 Ca (apfu). For comparison, the values of α_{Gl} and W_{TrGl} reported by Diener and Powell (2012) are 0.8 and 65 kJ, respectively, which were extracted from observed amphibole assemblages in natural rocks.

An attempt was made in this study to extract absolute values of the enthalpy of mixing directly from the $\delta\Delta Corr$ values using the method proposed by Etzel and Benisek (2008). These authors found that the change in the ΔH^{mix} (normalized to one atom per formula) with change in $\delta\Delta Corr$, i.e. a slope value, against the integrated excess volume of mixing produced consistent trends for a variety of silicate mineral joins with known enthalpies of mixing. Combining integrated excess volumes for the tremolite-glaucophane join from Jenkins et al. (2013) with the $\delta\Delta Corr$ values from this study over the three frequency ranges that were used by Etzel and Benisek (2008) produced maximum values of ΔH^{mix} that were in the range of 14 – 75 kJ. Even the lowest values will lead to unrealistically high critical-point temperatures (~ 4000°C). At present it appears that a universal relationship between ΔH^{mix} and autocorrelation values remains an important but elusive goal.

Implications

Liou and Maruyama (1987) provided one of the first diagrams representing the miscibility gap between actinolite and glaucophane based on their study of metabasites from Ward Creek in the Cazadero quadrangle, California. Their diagram did not include specific temperatures but rather indicated the general sense of increasing temperature with metamorphic facies. What is particularly noteworthy about their diagram is its symmetrical nature, if not the opposite sense of solvus asymmetry to that found in this study. This may be related to the high ferric-iron contents of these samples. Reynard and Ballèvre (1988) combined their investigation of coexisting actinolite and glaucophane occurring in eclogitic metagabbros from the Aosta Valley, Western Alps, with amphibole analyses in previous publications to produce the first quantitative actinolite-glaucophane miscibility gap. Their boundary is reproduced as the dash-dot curve in Figure 11 and compared with the two boundaries proposed in this study (Figure 4). Although the sense of asymmetry agrees with that found in this study, there is at least a difference of 150°C between the lower-temperature boundary (dotted curve) reported here and that of Reynard and Ballèvre (1988). Assuming the temperature estimates from the metamorphic parageneses are correct, this temperature discrepancy between the natural and synthetic analogues may be related to the iron in the natural samples. In the case of the Aosta Valley samples, the ferrous-iron number [$(Fe^{2+}/(Fe^{2+} + Mg) = Fe\#$] falls between 0.19 – 0.34 which might account for the differences in the critical-point temperatures.

In both the studies of Liou and Maruyama (1987) and Reynard and Ballèvre (1988) the evidence for a miscibility gap rested primarily on the presence of coexisting amphiboles without unequivocal textural evidence for exsolution. Such evidence was finally provided by Smelik and Veblen (1992) who documented the presence of coherent exsolution lamellae using transmission and analytical electron microscopy in Ca-rich glaucophane samples from various localities in

455 Vermont and California. Direct analyses of these fine-scale lamellar intergrowths were often
456 complicated by contributions from the host but, in general, supported the same sense of
457 miscibility-gap asymmetry as reported here, namely skewed toward Gl-rich compositions. Using
458 the electron microprobe analyses of coexisting actinolite (ave. Ca = 1.47(7) apfu) and
459 glaucophane (ave. Ca = 0.09(2) apfu) from Eclogite Brook, Vermont, reported by Smelik and
460 Veblen (1992), one would estimate a temperature of about 525 ±15 °C using the higher-
461 temperature miscibility gap (solid curve) in Figure 11, which is close to the 540-590°C
462 temperature range determined from garnet-omphacite pairs for this locality (Smelik and Veblen,
463 1992). In view of this agreement and the presence of significant Fe^{2+} (Fe# ~ 0.33) in the
464 Eclogite Brook samples, it may be that iron is not the primary cause for the difference between
465 the curves of Reynard and Ballèvre (1988) and this study. Experimental investigation of the
466 effect of iron on the location of this miscibility gap would be of considerable interest.
467 One other implication of this study is how it can help shed light on interpreting whether
468 complexly zoned or intergrown amphiboles represent equilibrium compositions among
469 immiscible amphiboles or are unrelated episodes of amphibole growth. The very Mg-rich
470 glaucophane occurring in the complex sodic and sodic-calcic assemblages of the amphibole
471 felses associated with the jadeitites from Pharkan, Myanmar, reported by Shi et al. (2003, 2012)
472 are particularly appropriate for this study. One of the questions raised by Shi et al. (2003) is
473 whether there was in fact a miscibility gap between glaucophane and winchite. For the
474 glaucophane occurring in the amphibole—Cr-cpx rock (sample C) with Ca contents of 0.15-0.38
475 apfu, one would expect coexisting winchite to have Ca contents ranging from a minimum of 0.75
476 up to about 1.2 apfu based on either the solid or dotted curves from this study in Figure 11.
477 These Ca contents are at least twice what is observed for the winchite occurring in this sample

(0.38 apfu) and confirms that the glaucophane and low-Ca-contented winchite in this sample do not share a miscibility gap as suggested by Shi et al. (2003).

Given the experimental difficulties of investigating coexisting amphibole assemblages because of the relatively low temperatures involved and the complex compositions of amphibole end members, it is suggested that the approach demonstrated in this study, namely combining the broad constraints of compositional re-equilibration experiments with the highly sensitive information on lattice strain afforded by autocorrelation analysis of infrared spectra, may prove to be a valuable approach in the future investigation of mineral miscibility studies.

Acknowledgments

Financial support for this project from the NSF grant EAR-0947175 to DMJ is gratefully acknowledged. Assistance with the electron microprobe images was provided by Mr. David Collins.

References Cited

Andrut, M., Gottschalk, M., Melzer, S., and Najorka, J. (2000) Lattice vibrational modes in synthetic tremolite-Sr-tremolite and tremolite-richterite solid solutions. Physics and Chemistry of Minerals, 27, 301-309.

Boffa Ballaran, T. and Carpenter, M. A. (2003) Line broadening and enthalpy: some empirical calibrations of solid solution behaviour from IR spectra. Phase Transitions, 76, 137-154.

Carpenter, M. A., Boffa Ballaran, T., and Atkinson, A. J. (1999) Microscopic strain, local structural heterogeneity and the energetics of silicate solid solutions. Phase Transitions, 69, 95-109.

Dale, J., Powell, R., White, R. W., Elmer, F. L., and Holland, T. J. B. (2005) A thermodynamic model for Ca-Na clinoamphiboles in Na_2O-CaO-FeO-MgO-Al_2O_3-SiO_2-H_2O-O for

petrological calculations. Journal of Metamorphic Geology, 23, 771-791.

Diener, J. F. A., Powell, R., White, R. W., and Holland, T. J. B. (2007) A new thermodynamic model for clino- orthoamphiboles in the system Na_2O-CaO-FeO-MgO-Al_2O_3-SiO_2-H_2O-O. Journal of Metamorphic Geology, 25, 631-656.

Diener, J. F. A. and Powell, R. (2012) Revised activity-composition models for clinopyroxene and amphibole. Journal of Metamorphic Geology, 30, 131-142.

Etzel, K., and Benisek, A. (2008) Thermodynamic mixing behavior of synthetic Ca-Tschermak-diopside pyroxene solid solutions: III. An analysis of IR line broadening and heat of mixing behavior. Physics and Chemistry of Minerals, 35, 399-407.

Goldsmith, J. R., and Heard, H. C. (1961) Subsolidus phase relations in the system $CaCO_3$-$MgCO_3$. Journal of Geology, 69, 45-74.

Hawthorne, F.C. and Grundy, H. D. (1976) The crystal chemistry of the amphiboles: IV. X-ray and neutron refinements of the crystal structure of tremolite. Canadian Mineralogist, 14, 334-345.

Hill, R. J., and Flack, H. D. (1987) The use of the Durbin-Watson *d* statistic in Rietveld analysis. Journal of Applied Crystallography, 20, 356-361.

Himmelberg, G. R. and Papike, J. J. (1969) Coexisting amphiboles from blueschist facies metamorphic rocks. Journal of Petrology, 10, 102-114.

Hofmeister, A. M., and Bowey, J. E. (2006) Quantitative infrared spectra of hydrosilicates and related minerals. Monthly Notices of the Royal Astronomical Society, 367, 577-591.

Holland, T. and Powell, R. (2003) Activity-composition relations for phases in petrological calculations: an asymmetric multicomponent formulation. Contributions to Mineralogy and Petrology, 145, 492-501.

524 Holmes, Z. F., Jenkins, D. M., and Ishida, K. (2012) Autocorrelation analysis of the IR spectra of
525 synthetic carbonates along the calcite-dolomite join. Geological Society of America,
526 Abstracts with Programs, 44(7), 494, Abstract 207-9.
527 Hovis, G. L., Delbove, F., and Bose, M. R. (1991) Gibbs energies and entropies of K-Na mixing
528 for alkali feldspars from phase equilibrium data: Implications for feldspar solvi and short-
529 range order. American Mineralogist, 76, 913-927.
530 Ishida, K., Jenkins, D. M., and Hawthorne, F. C. (2008) Mid-IR bands of synthetic calcic
531 amphiboles of tremolite-pargasite series and of natural calcic amphiboles. American
532 Mineralogist, 93, 1112-1118.
533 Jenkins, D.M. (1987) Synthesis and characterization of tremolite in the system
534 H_2O-CaO-MgO-SiO_2. American Mineralogist, 72, 707-715.
535 Jenkins, D.M. (1994) Experimental reversal of the aluminum content in tremolitic amphiboles in
536 the system H_2O-CaO-MgO-Al_2O_3-SiO_2. American Journal of Science, 294:593-620.
537 Jenkins, D. M., Della Ventura, G., Oberti, R., and Bozhilov, K. (2013) Synthesis and
538 characterization of amphiboles along the tremolite–glaucophane join. American
539 Mineralogist, 98, 580-600.
540 Koch-Müller, M., Mrosko, M., Gottschalk, M., and Schade, U. (2012) Pressure-induced phase
541 transitions in ilvaite studied by *in situ* micro-FTIR. European Journal of Mineralogy, 24, 831-
542 838.
543 Larson, A. C. and Von Dreele, R. B. (2000) General Structure Analysis System (GSAS). Los
544 Alamos National Laboratory Report LAUR 86-748.
545 Levien, L., Prewitt, C. T., and Weidner, D. J. (1980) Structure and elastic properties of quartz at
546 pressure. American Mineralogist, 65, 920-930.

547 Liou, J. G. and Maruyama, S. (1987) Parageneses and compositions of amphiboles from
548 Franciscan jadeite-glaucophane type facies series metabasites at Cazadero, California.
549 Journal of Metamorphic Geology, 5, 371-395.
550 Maresch, W. V., Medenbach, O., and Rudolph, A. (1982) Winchite and the actinolite-
551 glaucophane miscibility gap. Nature, 296, 731-732.
552 Navrotsky, A. and Capobianco, C. (1987) Enthalpies of formation of dolomite and of magnesian
553 calcites. American Mineralogist, 72, 782-787.
554 Nestola, F., Gatta, G. D., and Boffa Ballaran, T. (2006) The effect of Ca substitution on the
555 elastic and structural behavior of orthoenstatite. American Mineralogist, 91, 809-815.
556 Ohashi, Y. (1984) Polysynthetically-twinned structures of enstatite and wollastonite. Physics
557 and Chemistry of Minerals, 10, 217-229.
558 Papike, J. J. and Clark, J. R. (1968) The crystal structure and cation distribution of glaucophane.
559 American Mineralogist, 53, 1156-1173.
560 Pavese, A., Bocchio, R., and Ivaldi, G. (2000) In situ high temperature single crystal X-ray
561 diffraction study of a natural omphacite. Mineralogical Magazine, 64, 983-993.
562 Perdikatsis, B. and Burzlaff, H. (1981) Structurverfeinerung am Talk $Mg_3[(OH)_2Si_4O_{10}]$.
563 Zeitschrift für Kristallographie, 156, 177-186.
564 Reynard, B., and Ballèvre, M. (1988) Coexisting amphiboles in an eclogite from the Western
565 Alps: new constraints on the miscibility gap between sodic and calcic amphiboles. Journal
566 of Metamorphic Geology, 6, 333-350.
567 Salje, E. K. H., Carpenter, M. A., Malcherek, T. G. W., and Boffa Ballaran, T. (2000)
568 Autocorrelation analysis of infrared spectra. European Journal of Mineralogy, 12, 503-519.
569 Shi, G.-H., Cui, W.-Y., Tropper, P., Wang, C.-Q., Shu, G.-M., and Yu, H. (2003) The petrology

of a complex sodic and sodic-calcic amphibole association and its implications for the metasomatic processes in the jadeitite area in northwestern Myanmar, formerly Burma. Contributions to Mineralogy and Petrology, 145, 355-376.

Shi, G., Harlow, G. E., Wang, Jing, Wang, Jun, Ng, E., Wang, Xia, Cao, S., and Cui, W. (2012) Mineralogy of jadeitite and related rocks from Myanmar: a review with new data. European Journal of Mineralogy, 24, 345-370.

Smelik, E. A. and Veblen, D. R. (1992) Exsolution of Ca-amphibole from glaucophane and the miscibility gap between sodic and calcic amphiboles. Contributions to Mineralogy and Petrology, 112, 178-195.

Sokolova, E. V., Hawthorne, F. C., Gorbatova, V., McCammon, C., Schneider, J. (2001) Ferrian winchite from the Ilmen Mountains, southern Urals, Russia, and some problems with the current scheme for amphibole nomenclature. Canadian Mineralogist, 39, 171-177.

Spear, F. S. (1995) Metamorphic phase equilibria and pressure-temperature-time paths, Monograph, 799 p. Mineralogical Society of America, Washington, DC.

Tarantino, S. C., Boffa Ballaran, R., Carpenter, M. A., Domeneghetti, M. C., and Tazzoli, V. (2002) Mixing properties of the enstatite-ferrosilite solid solution: II. A microscopic perspective. European Journal of Mineralogy, 14, 537-547.

Tarantino, S. C., Carpenter, M. A., and Domeneghetti, M. C. (2003) Strain and local heterogeneity in the forsterite-fayalite solid solution. Physics and Chemistry of Minerals, 30, 495-502.

590

591 Table 1. Compositions of phases and oxide/hydroxide mixtures used in this study, the conditions
592 of synthesis, and products of synthesis.

Sample Code	Composition	*T* (°C)	*P* (GPa)	t (h)	added H_2O (wt%)	Products*
FEGL-5 mix	$Na_2Mg_3Al_2Si_8O_{22}(OH)_2$ = Gl	----	----	----	----	Na-Al-Si-oxide, $Mg(OH)_2$ mixture
FEGL 5-2-7**	$Na_2Mg_3Al_2Si_8O_{22}(OH)_2$ = Gl	750(10)	2.5(1)	891	4.4(1)	amph, qtz,(talc)
WIN 11-3	$(Na_{1.2}Ca_{0.8})(Mg_{3.8}Al_{1.2})Si_8O_{22}(OH)_2$ = $Tr_{40}Gl_{60}$	780(10)	1.97(6)	334	4.2(1)	amph, qtz, liq
TREM-26 mix	$Ca_{1.90}Mg_{5.10}Si_8O_{22}(OH)_2$ = $Tr_{95}Mc_{05}$ §	----	----	----	----	$Ca(OH)_2$, $Mg(OH)_2$, SiO_2 mixture
TREM 23-13	$(Ca_{1.8}Mg_{5.2})Si_8O_{22}(OH)_2$ = $Tr_{90}Mc_{10}$§	801(5)	0.452(5)	458	30(1)	amph, (qtz), (cpx)
OMPH 1-1	$(Na_{0.5}Ca_{0.5})(Al_{0.5}Mg_{0.5})Si_2O_6$	700(10)	1.57(5)	47	2.5(4)	omphacite
TALC 1-1	$Mg_3Si_4O_{10}(OH)_2$	605(5)	0.20(1)	120	30(1)	talc, (qtz)

593 Note: Abbreviations: amph = amphibole; cpx = diopsidic clinopyroxene; liq = silicate liquid or
594 quenched solute; qtz = quartz.
595 *Phases in parentheses represent minor phases (< 5 wt%)
596 ** This sample was treated seven separate times, with intermediate grinding, for the total
597 duration shown to react out the intermediate phases jadeite and smectite.
598 §Bulk compositions were intentionally enriched in 5 or 10 mol% of the $Mg_7Si_8O_{22}(OH)_2$ (= Mc)
599 component and ~4 wt% SiO_2 to maximize the yield of amphibole and minimize diopsidic
600 clinopyroxene and dissolution of silica (e.g., Jenkins, 1987).
601

602

603 Table 2. Starting mixtures used in this study

Phase (code)	Mixture code				
	GLTR - 2	GLTR - 3	GLTR - 4	GLTR - 5	GLTR - 6
Glaucophane (FEGL 5-2-7)	X	----	X	----	----
Glaucophane mix* (FEGL-5 mix)	----	----	----	----	X
Tremolite (TREM 23-13)	X	X	----	----	----
Tremolite mix** (TREM-26)	----	----	----	X	----
Winchite (WIN 11-3)	----	----	----	X	X
Omphacite (OMPH 1-1)	----	X	X	----	----
Talc (TALC 1-1)	----	X	X	----	----
Bulk composition	$Tr_{45}Mc_5Gl_{50}$	$Tr_{54}Mc_6Gl_{40}$	$Tr_{36}Mc_4Gl_{60}$	$Tr_{50}Mc_1Gl_{49}$	$Tr_{30}Gl_{70}$

604 *Mixture of Na_2CO_3, Al_2O_3, SiO_2 and $Mg(OH)_2$ of Gl_{100} ($+H_2O$) bulk composition, prepared by

605 mixing the first three reagents, decarbonating at 900°C, then adding $Mg(OH)_2$.

606 ** Mixture of $Ca(OH)_2$, $Mg(OH)_2$, and SiO_2 of the bulk composition $Tr_{95}Mc_{05}$ ($+ H_2O$).

607 Table 3. Compositional re-equilibration experiments

Sample Code	*T* (°C)	*P* (GPa)	t (h)	added H_2O (wt%)	Products*
GLTR 2-1	500(5)	1.58(5)	138	2.1(4)	trem, glauc, qtz
GLTR 2-2	600(5)	1.62(5)	424	1.8(6)	trem, glauc, qtz, (talc)
GLTR 2-6	650(5)	1.83(8)	190	2.3(12)	trem, glauc, qtz, (talc)
GLTR 2-3	700(5)	1.60(4)	208	2.4(4)	trem, glauc, qtz, (talc)
GLTR 2-3-2**	700(5)	1.59(5)	290	1.6(4)	trem, glauc, qtz
GLTR 2-3-3**	700(5)	1.61(5)	172	4.2(14)	trem, glauc, qtz
GLTR 2-7-1	750(10)	1.59(5)	141	1.9(4)	amph, talc, (qtz)
GLTR 2-8	750(5)	1.60(4)	209	1.9(2)	trem, glauc, (qtz), (talc)
GLTR 2-8-2**	750(5)	1.60(6)	208	2.6(5)	trem, glauc, qtz
GLTR 2-8-3**	750(5)	1.62(5)	216	2.4(4)	trem, qtz
GLTR 2-4	800(5)	1.60(4)	120	1.7(5)	trem, glauc, qtz
GLTR 2-4-2**	800(5)	1.55(7)	168	3.5(18)	amph, qtz, (plagioclase)
GLTR 3-1	600(5)	1.62(5)	234	3.9(9)	omph, talc, trem, qtz
GLTR 4-1	600(5)	1.62(5)	234	2.4(8)	omph, talc, glauc, qtz
GLTR 3-2	700(5)	1.62(6)	190	2.7(5)	trem, omph, talc, qtz
GLTR 4-2	700(5)	1.62(6)	190	2.6(5)	trem, glauc, talc, qtz
GLTR 3-3	800(5)	1.62(6)	88	2.9(14)	amph, enst
GLTR 4-3	800(5)	1.62(6)	88	3.4(6)	amph, clino-enst

GLTR 5-1	500(5)	1.79(6)	484	0	amph, qtz, omph, (talc)
GLTR 6-1	500(5)	1.79(6)	484	0	amph, glauc, qtz
GLTR 5-2	550(5)	1.88(10)	170	0	amph, qtz, omph, (talc)
GLTR 6-2	550(5)	1.88(10)	170	0	amph, glauc, qtz
GLTR 5-3	600(5)	1.82(5)	192	0	amph, qtz, omph, (talc)
GLTR 6-3	600(5)	1.82(5)	192	0	amph, glauc, qtz
GLTR 5-4	650(5)	1.82(5)	215	0	amph, qtz, omph, (talc)
GLTR 6-4	650(5)	1.82(5)	215	0	amph, glauc, qtz
GLTR 5-5	700(5)	1.82(6)	116	0	amph, qtz, (omph)
GLTR 6-5	700(5)	1.82(6)	116	0	amph, glauc, qtz
GLTR 5-6	750(5)	1.82(4)	120	0	amph, qtz
GLTR 6-6	750(5)	1.82(4)	120	0	amph, glauc, qtz

608 Note: Abbreviations: amph = winchite-rich amphibole; clino-enst = clino-enstatite; enst =
609 enstatite; glauc = glaucopane-rich amphibole; omph = omphacite; trem = tremolite-rich
610 amphibole; qtz = quartz.
611 *Phases in parentheses are present at minor levels (< 5 wt%).
612 **Retreatment of the preceeding experiment.
613
614

615 Table 4. Electron microprobe analyses of starting-material amphiboles used in the mixtures
616 listed in Table 3. Starting-material amphiboles have the nominal mol% Gl contents indicated
617 and values are averages of *n* analyses. Uncertainties in last digit are shown in parentheses.

Sample Code	TREM 23-13 0% Gl	FEGL 5-2-7 100% Gl	WIN 11-3 60% Gl
n	9	14	15
weight%			
SiO_2	42.8(17)	51.8(88)	56.9(10)
Al_2O_3	----	11.6(19)	7.3(16)
MgO	18.8(9)	13.3(21)	22.4(8)
CaO	8.8(7)	0.12(4)	6.1(6)
Na_2O	----	6.7(11)	4.6(4)
Total	70.5(28)	83(14)	97.3(4)
cations			
Si	7.99(5)	7.91(9)	7.64(13)
^{T}Al	----	0.09(9)	0.35(13)
^{C}Al	----	1.99(8)	0.80(13)
^{C}Mg	5.00	2.99(11)	4.20(13)
^{B}Mg	0.25(13)	0.04(4)	0.29(6)
^{B}Ca	1.76(14)	0.02(1)	0.88(8)
^{B}Na	----	1.91(9)	0.83(6)
^{A}Na	----	0.08(9)	0.38(7)
Total	15.01(6)	15.04(13)	15.38(7)

618
619

620 Table 5. Calcium contents on the B sites of starting-material amphiboles and of amphiboles in
621 GLTR 2-, 3-, 4-, 5-, and 6-series experiments derived from unit-cell volumes of experimental
622 products.

Sample Code	Tr-rich amphibole		Gl-rich amphibole	
	V (Å^3)	^{B}Ca (apfu)	V (Å^3)	^{B}Ca (apfu)
TREM 23-13	903.38(7)	1.61(9)	----	----
FEGL 5-2-7	----	----	866.52(9)	0.03(1)
WIN 11-3	892.95(6)	0.92(8)	----	----
GLTR 2-1	904.2(2)	1.72(7)	866.5(1)	0.03(1)
GLTR 2-2	903.4(2)	1.61(8)	866.9(1)	0.04(2)
GLTR 2-6	903.4(3)	1.61(8)	867.3(2)	0.05(2)
GLTR 2-3	901.5(2)	1.42(9)	866.4(3)	0.03(1)
GLTR 2-3-2	898.8(2)	1.23(9)	870.8(5)	0.15(2)
GLTR 2-3-3	897.5(2)	1.15(9)	868.6(6)	0.09(2)
GLTR 2-7-1	897.8(1)	1.17(9)	----	----
GLTR 2-4	898.3(1)	1.20(9)	869.8(10)	0.12(2)
GLTR 2-4-2	896.8(1)	1.11(9)	----	----
GLTR 2-8	898.8(2)	1.23(9)	871.1(4)	0.16(2)
GLTR 2-8-2	895.5(2)	1.04(9)	872.9(7)	0.21(3)
GLTR 2-8-3	895.8(1)	1.06(8)	----	----
GLTR 3-1	903.7(4)	1.65(8)	----	----
GLTR 3-2	899.5(2)	1.28(9)	----	----

GLTR 3-3	902.6(1)	1.52(9)	----	----
GLTR 4-1	----	----	866.4(3)	0.03(2)
GLTR 4-2	896.6(1)	1.10(9)	866.8(3)	0.04(2)
GLTR 4-3	899.3(1)	1.26(9)	----	----
GLTR 5-1	892.4(1)	0.89(8)	----	----
GLTR 5-2	892.5(1)	0.90(8)	----	----
GLTR 5-3	892.8(1)	0.91(8)	----	----
GLTR 5-4	892.8(1)	0.91(8)	----	----
GLTR 5-5	893.4(1)	0.94(8)	----	----
GLTR 5-6	893.8(1)	0.96(8)	----	----
GLTR 6-1	892.1(1)	0.88(8)	871.0(4)	0.15(2)
GLTR 6-2	891.4(1)	0.85(7)	872.3(4)	0.19(3)
GLTR 6-3	891.1(1)	0.83(7)	872.8(3)	0.20(3)
GLTR 6-4	891.6(1)	0.85(7)	875.2(3)	0.27(3)
GLTR 6-5	892.4(2)	0.89(8)	879.4(2)	0.40(4)
GLTR 6-6	891.9(2)	0.87(7)	880.2(3)	0.43(4)

623
624

Table 6. Summary of some properties of synthetic amphiboles made from mixtures along the tremolite-glaucophane join reported by Jenkins et al. (2013).

Sample Code	Nom. Gl (mol%)	Nom. Ca ($^{B}X_{Ca}$)	Obs. Ca* ($^{B}X_{Ca}$)	V (Å^3)	Calc. Ca** ($^{B}X_{Ca}$)
TREM 26-2	0	0.95	0.92(4)	903.4(1)	0.80(4)
WIN 7-1	10	0.90	0.84(3)	903.6(1)	0.82(4)
WIN 8-1	20	0.80	0.79(4)	904.4(1)	0.87(3)
WIN 9-1	30	0.70	0.71(2)	901.38(9)	0.71(5)
WIN 10-1	40	0.60	0.65(6)	899.57(8)	0.64(5)
WIN 1-1	50	0.50	0.54(6)	894.86(7)	0.50(4)
WIN 11-1	60	0.40	0.46(4)	894.00(8)	0.48(4)
WIN 12-2	70	0.30	0.34(5)	887.2(1)	0.34(3)
WIN 2-2	80	0.20	0.24(3)	883.1(1)	0.26(3)
WIN 13-3	90	0.10	0.11(3)	873.6(1)	0.11(2)
FEGL 5-3-4	100	0.00	0.01(1)	866.87(8)	0.02(1)

*Ca determined by electron microprobe analysis, reported by Jenkins et al. (2013)

**Ca calculated from the unit-cell volume using equation (1) in the text.

Figure Captions

Figure 1. Experimental approaches used to locate the tremolite-glaucophane miscibility gap. (a) Re-equilibration by mutual dissolution of tremolite (Tr) and glaucophane (Gl) for the starting mixture GLTR-2 having the bulk composition 2. (b) Enrichment of tremolite to a more Gl-rich composition by reaction with talc and omphacite (Omph) for starting mixture GLTR-3 (point 3). Enrichment of glaucophane to a more Tr-rich composition by reaction with Omph and talc for starting mixture GLTR-4 (point 4). (c) Compositional shift of an intermediate winchitic amphibole (WIN 11-3) either to a more Tr-rich composition by reaction with an oxide mixture of tremolite bulk composition (open circle Tr) for the starting mixture GLTR-5 (point 5), or to a more Gl-rich composition by reaction with an oxide mixture of glaucophane bulk composition (open circle Gl) for the starting mixture GLTR-6 (point 6). In most cases this compositional shift will be by the formation of overgrowths on seed crystals. All compositions are plotted as a projection onto the ternary diagram MgO-CaO-($NaO_{0.5}$+$AlO_{1.5}$) from SiO_2 and H_2O.

Figure 2. Compositional re-equilibration results for the GLTR 2-series experiments listed in Table 3. Open circles are the compositions of individual amphiboles determined by electron microprobe analysis. Solid circle shows the bulk composition of the starting mixture, while the solid squares are the compositions of the starting tremolite (TREM 23-13, Tr) and glaucophane (FEGL 5-2-7, Gl). Results are from (a) GLTR 2-1 at 500°C, (b) GLTR 2-2 at 600°C, (c) GLTR 2-3 at 700°C, and (d) GLTR 2-4 at 800°C. All treatments were at 1.6 GPa. Projection is from $Mg_7Si_8O_{22}(OH)_2$ and H_2O onto the ternary diagram ($NaO_{0.5}$+$AlO_{1.5}$)-CaO-SiO_2 which allows variations in the SiO_2 content of the amphibole to be shown.

Figure 3. Portions of the powder XRD patterns from the treatment of tremolite (Tr) and glaucophane (Gl) in the GLTR-2-series starting mixture (Mix) at 600, 700, and 800°C, listed

as samples GLTR 2-2, GLTR 2-3, and GLTR 2-4, respectively, in Table 3. These patterns show subtle changes in certain XRD peak positions, as for the 240 and 310, related to compositional changes in the amphiboles, and more obvious changes, as in the loss of a peak (e.g., 240 of Gl), related to the merging of two amphiboles into one (800°C).

Figure 4. Compositions of re-equilibrated amphiboles based on the volume-composition relations of equation (1). Vertical dashed lines represent the compositions of the starting-material amphiboles (from electron microprobe analysis) while the arrows indicate the sense of compositional re-equilibration. Solid circles are the results of the compositional re-equilibration of Gl-rich and Tr-rich amphiboles (GLTR-2-series, Table 5, Fig. 5), with the right-pointing arrows at 750 and 800°C showing the change to a single Tr-enriched amphibole. Open circles are the compositions of tremolite (GLTR-3-series, Table 5) and glaucophane (GLTR-4-series, Table 5) treated in the presence of omphacite and talc. Open squares are the compositions of Gl-rich amphiboles formed either as free-standing grains or overgrowing existing winchitic-amphibole seeds (GLTR-6-series, Table 5). The solid and dotted curves are the calculated miscibility gaps that satisfy both the experimental and autocorrelation analysis results of this study, as discussed in the text.

Figure 5. Amphibole dissolution time-series experiments. Circles are the results at 700° (GLTR 2-3-series), diamonds the results at 750° (GLTR 2-8-series), and squares the results at 800°C (GLTR 2-4-series) based on the data in Tables 3 and 5. Compositions were determined from the volume-composition relations of equation (1).

Figure 6. Back-scattered electron image of a portion of the products from treating winchitic amphibole in the presence of an oxide-hydroxide mixture of glaucophane bulk composition at 750°C, 1.82 GPa, for 120 h (GLTR 6-6, Table 3). This image shows lighter winchite-rich

678 cores (C) with slightly darker-grey glaucophane-rich rims (R, arrows). Quartz (Qtz) is also
679 present in this image. Scale bar is 10 μm.

680 Figure 7. (a) Mid-infrared absorption spectra of synthetic amphiboles formed from mixtures at
681 10 mol% increments along the tremolite-glaucophane join. Patterns are offset for clarity and
682 labeled with the nominal mol% Gl content. Numbered peaks indicate specific bands used to
683 model the spectra. (b) Far-infrared absorption spectra for the same samples.

684 Figure 8. (a) Band positions (cm^{-1}) with change in amphibole composition, represented here as
685 the mole fraction of Ca in the B or M(4) sites, for the mid-infrared spectra of Figure 7a. (b)
686 Band positions for the far-infrared spectra of Figure 7b. Numbers refer to the specific bands
687 in Figure 7.

688 Figure 9. Autocorrelation analysis of portions of the mid- and far-infrared spectra of amphiboles
689 formed along the tremolite-glaucophane join (Jenkins et al. 2013) and summarized in Table
690 6. The autocorrelation parameter ($\Delta Corr_i$) is plotted against the mole fraction of Ca in the B
691 or M(4) site ($^{B}X_{Ca}$). The portions of the spectra that were autocorrelated are as follows: (a)
692 850-1200 cm^{-1}, (b) 720-800 cm^{-1}, (c) 650-700 cm^{-1}, (d) 400-600 cm^{-1}, (e) 200-275 cm^{-1}, and
693 (f) 100-200 cm^{-1}. Curves are polynomial fits to the individual data points (circles) given only
694 to aid visualization, while the double-headed arrows indicate how $\delta\Delta Corr_i$ values are defined
695 relative to the linear baseline between end-member samples.

696 Figure 10. (a) – (f) Plots of $\delta\Delta Corr_i$ values, i.e., the excess value of $\Delta Corr$ over a linear
697 combination of the end-members, for the same frequency ranges shown in Figure 9. Solid
698 curves are calculated fits based on the asymmetric formalism theory of Holland and Powell
699 (2003) with the derived values of W_{Corr} and α_{Gl} using all of the data for each frequency range
700 given on the figure. Dotted curves are the same asymmetric formalism treatment but using

only the two most Gl-rich and three most Tr-rich samples of each region, as discussed in the text, with the associated values of α_{Gl} given in square brackets. Uncertainties (1σ) in the last digit are given in parentheses.

Figure 11. Solid and dotted curves are the miscibility gaps derived from this study based on the upper and lower ranges for W_{TrGl} of 70 and 67 kJ, respectively. The miscibility gap reported by Reynard and Ballèvre (1988) based on coexisting amphibole assemblages from the western Alps is shown for comparison as the dash-dot curve.

710 Figure 1

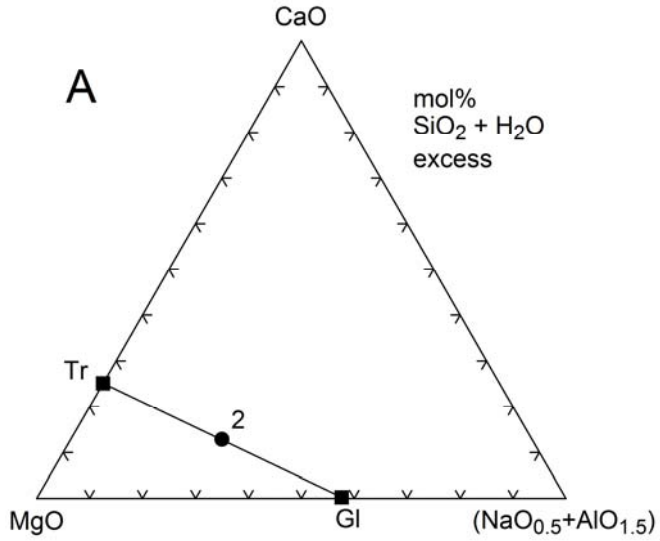

711
712

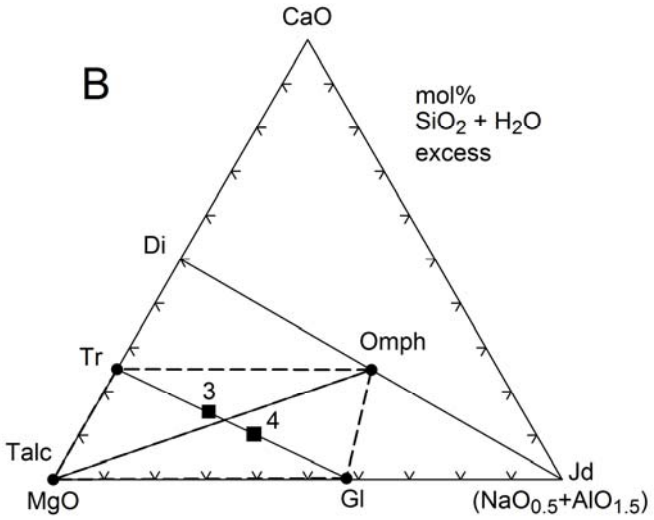

713
714

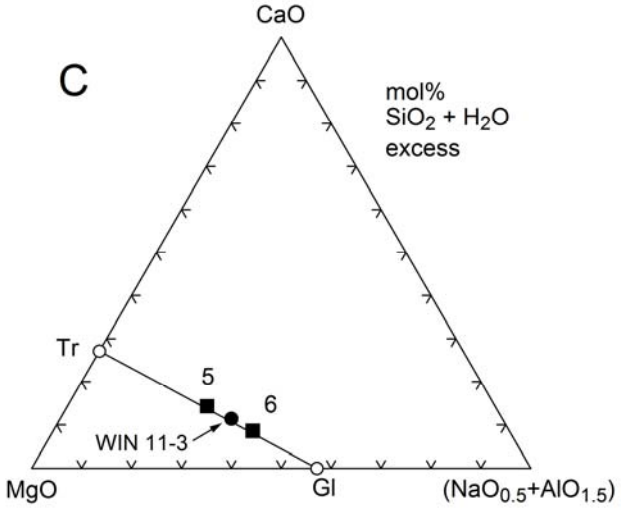

715

716

717 Figure 2

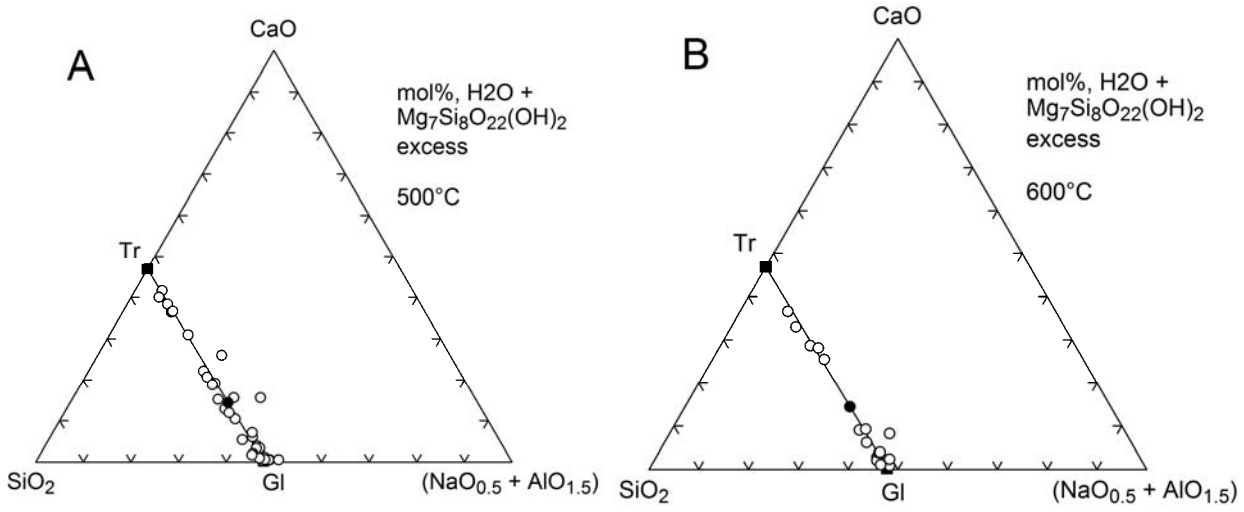

718

719

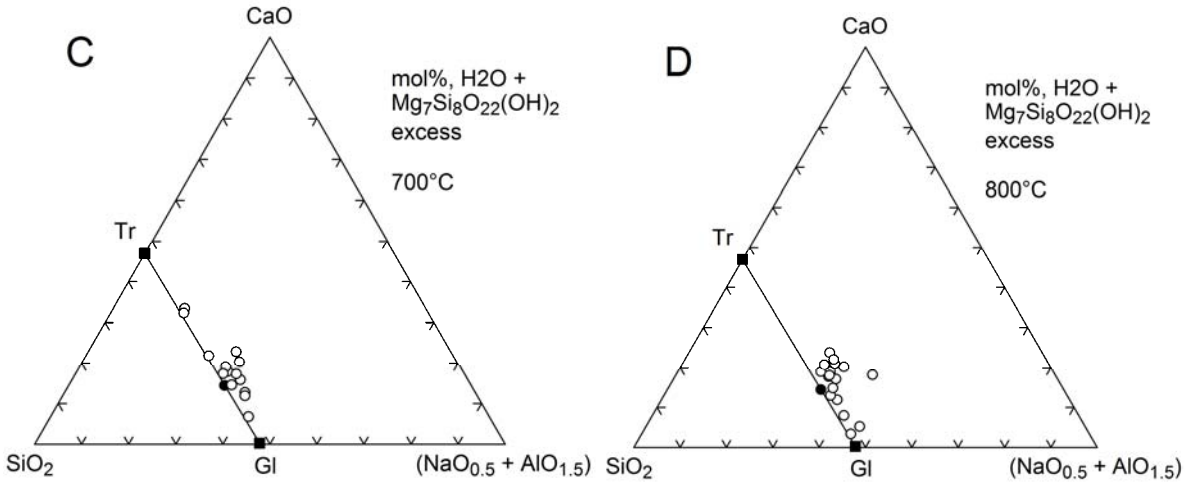

720

721

722 Figure 3

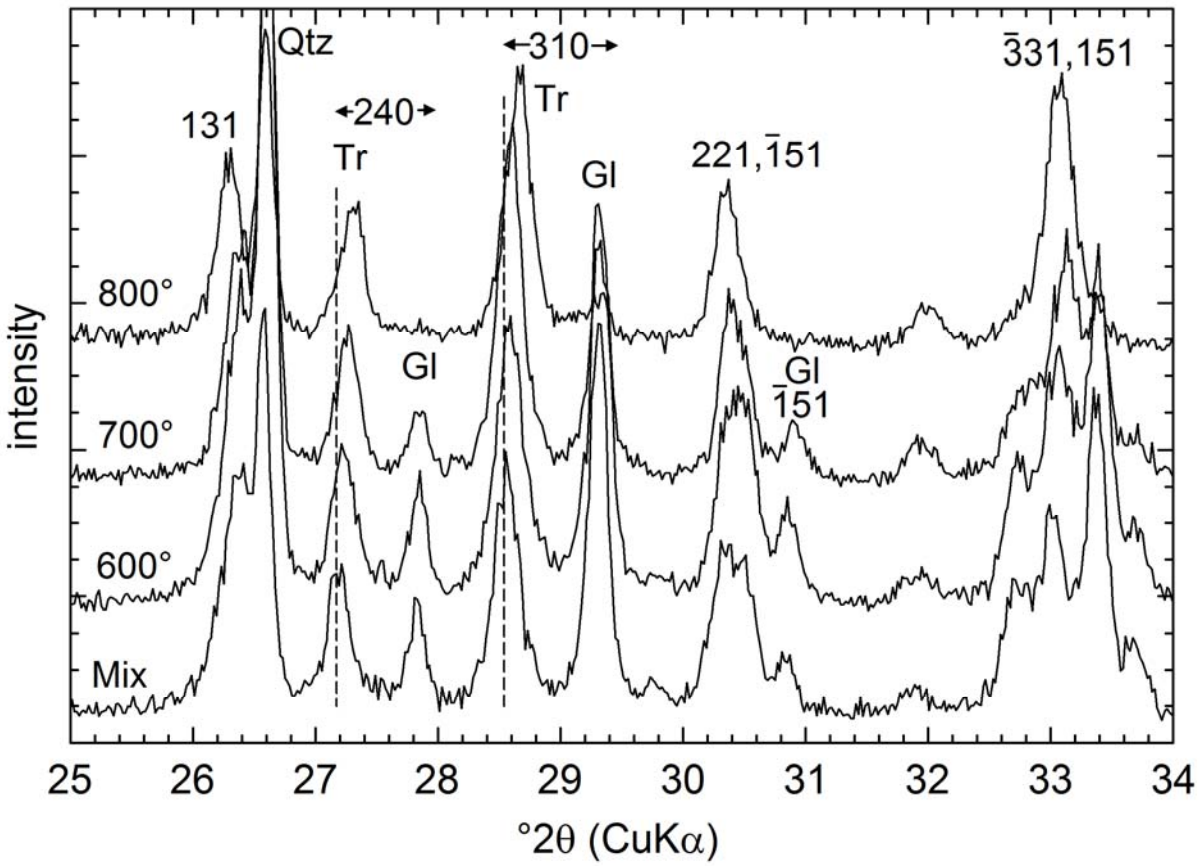

723
724
725

726

727 Figure 4

728

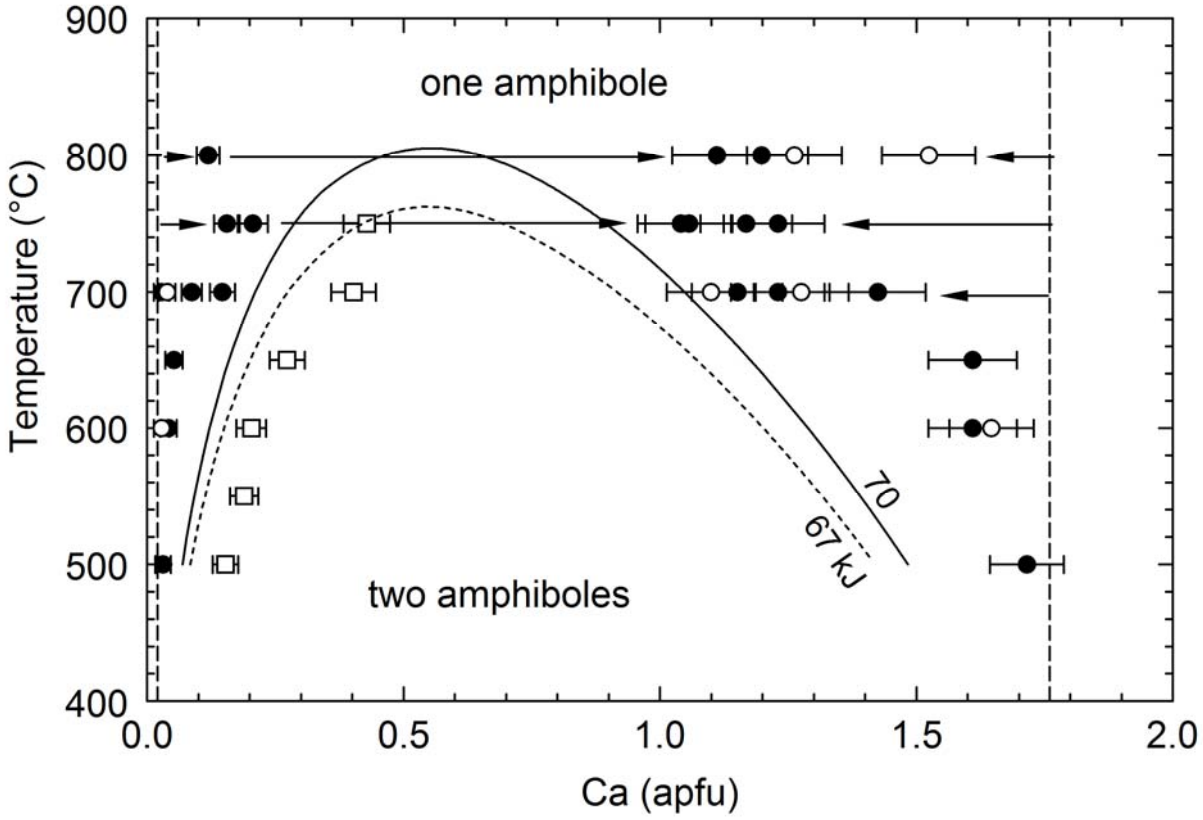

729

730

731

732 Figure 5

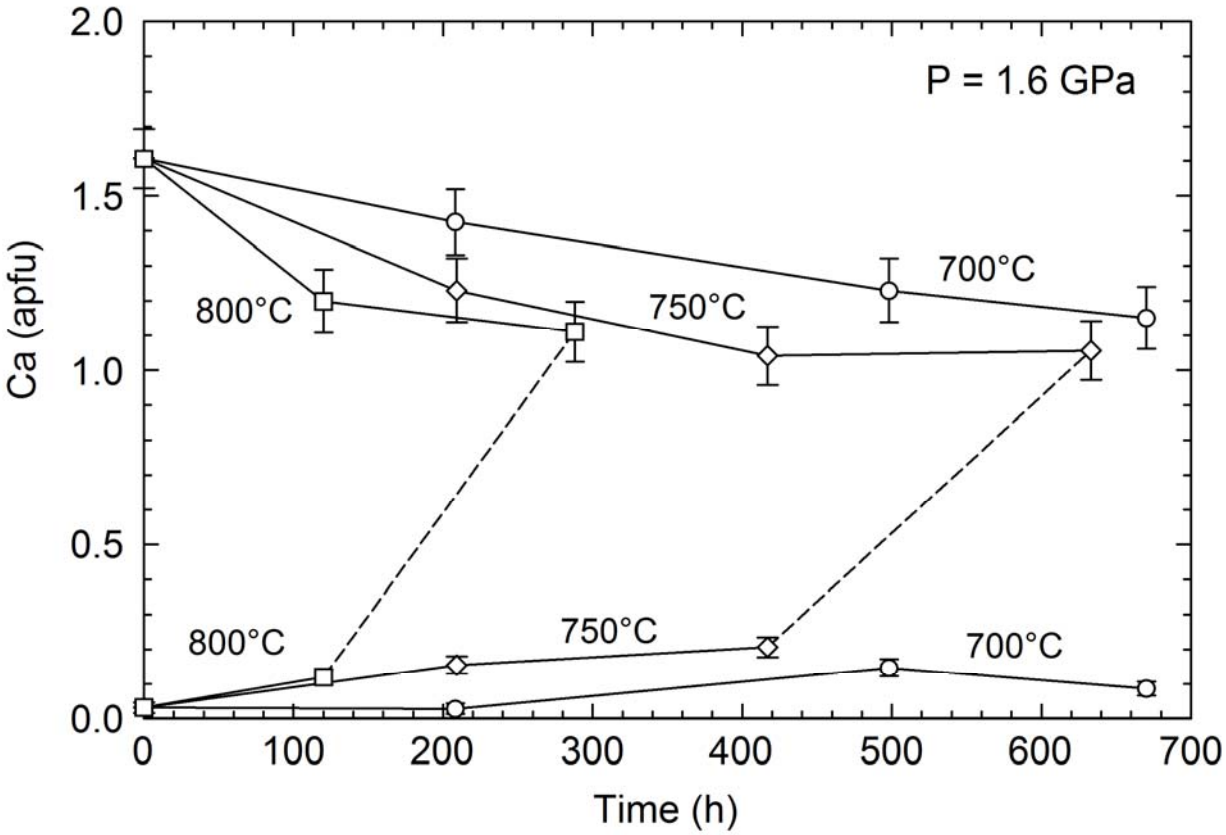

733

734

735

736 Figure 6

737

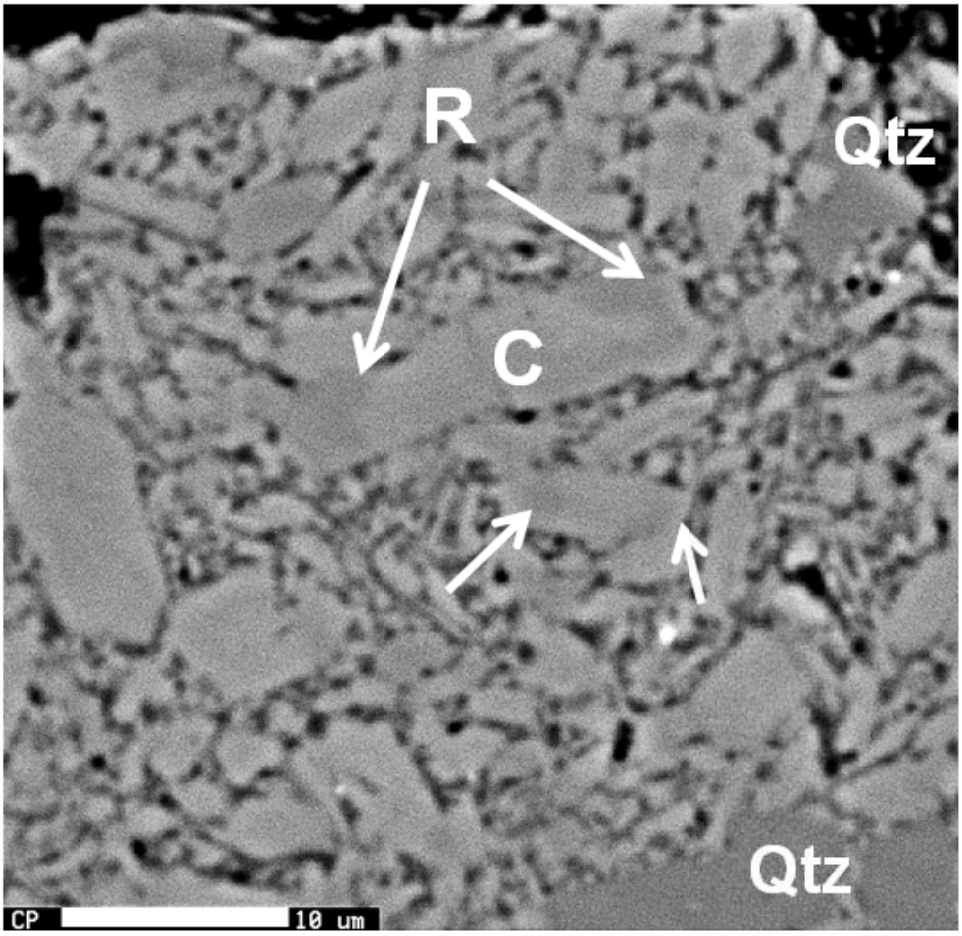

738

739

740

741 Figure 7

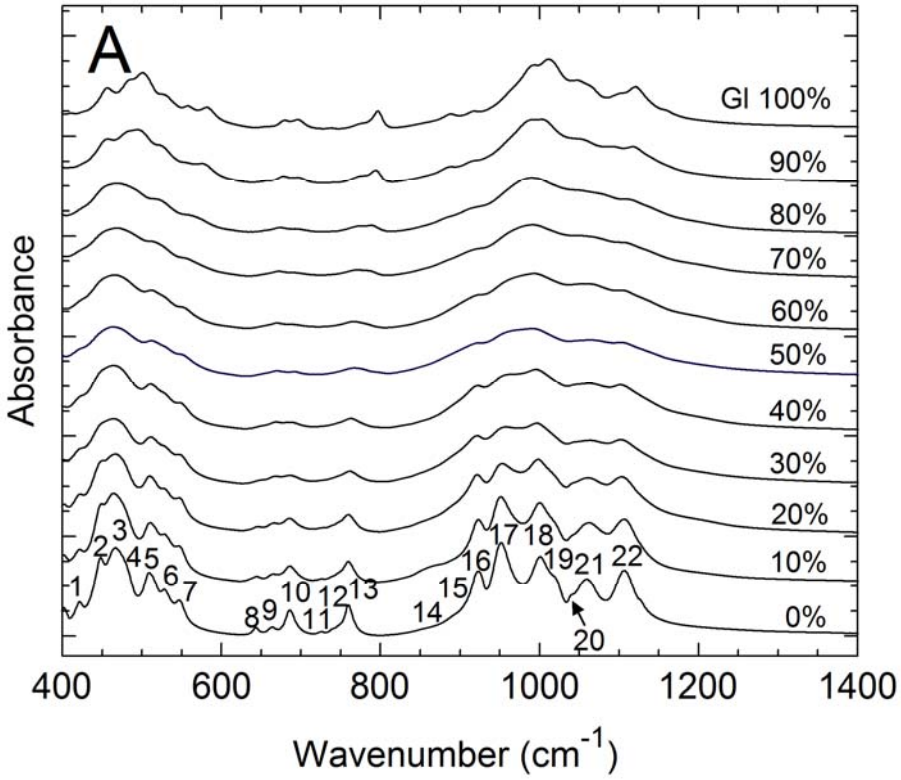

742
743

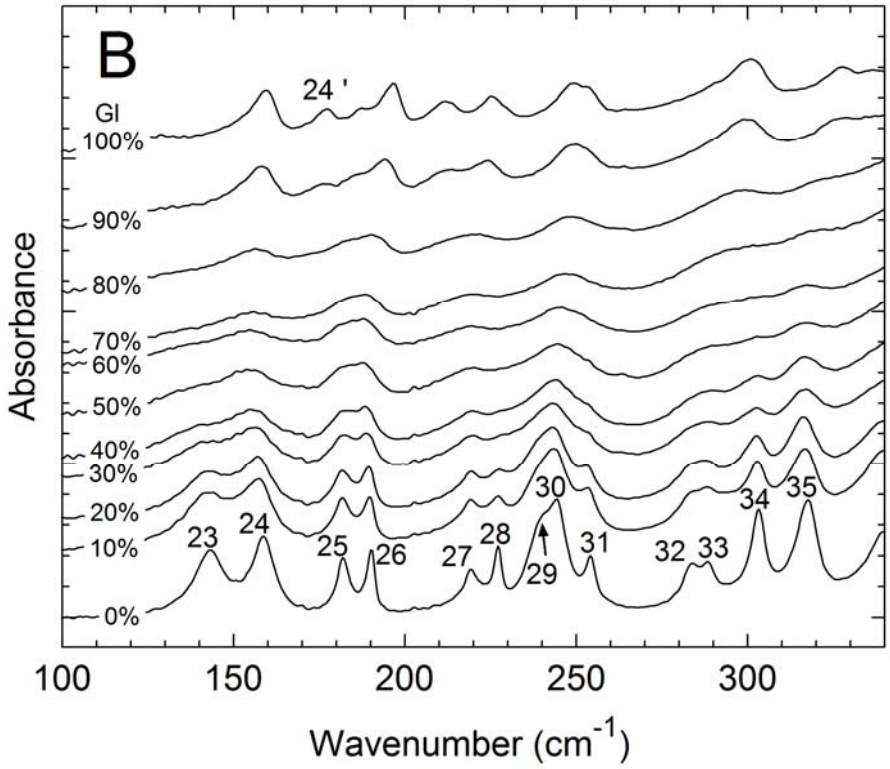

744
745

746 Figure 8
747

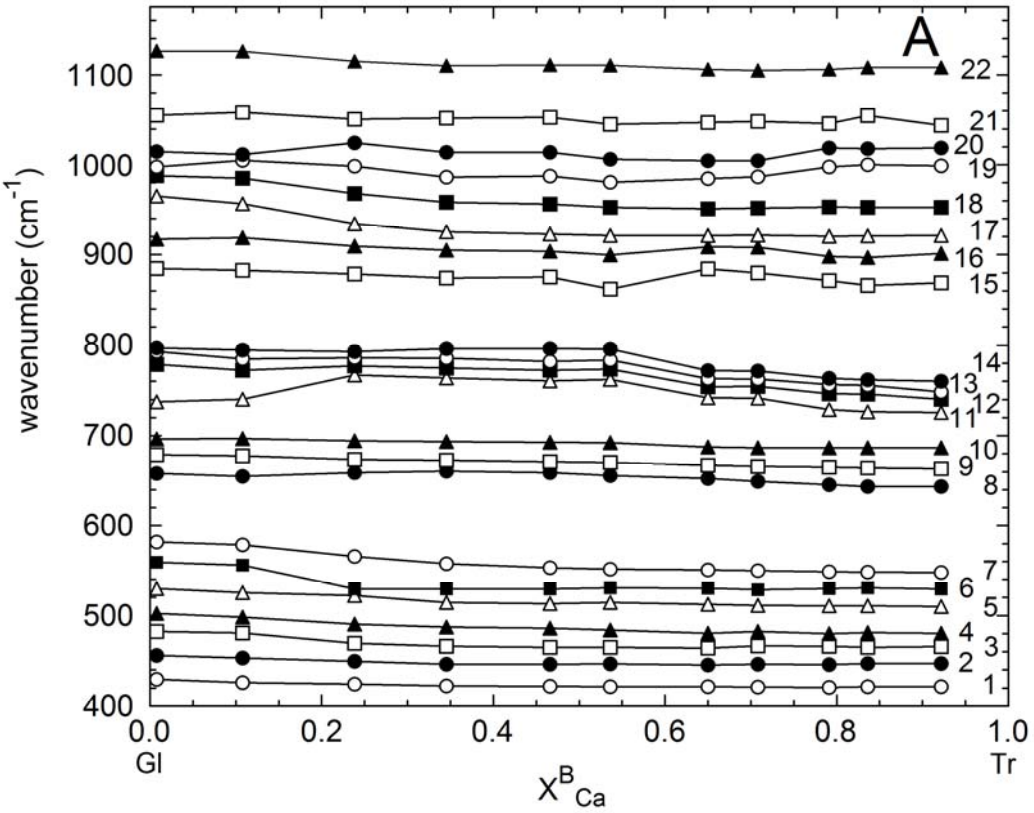

748
749

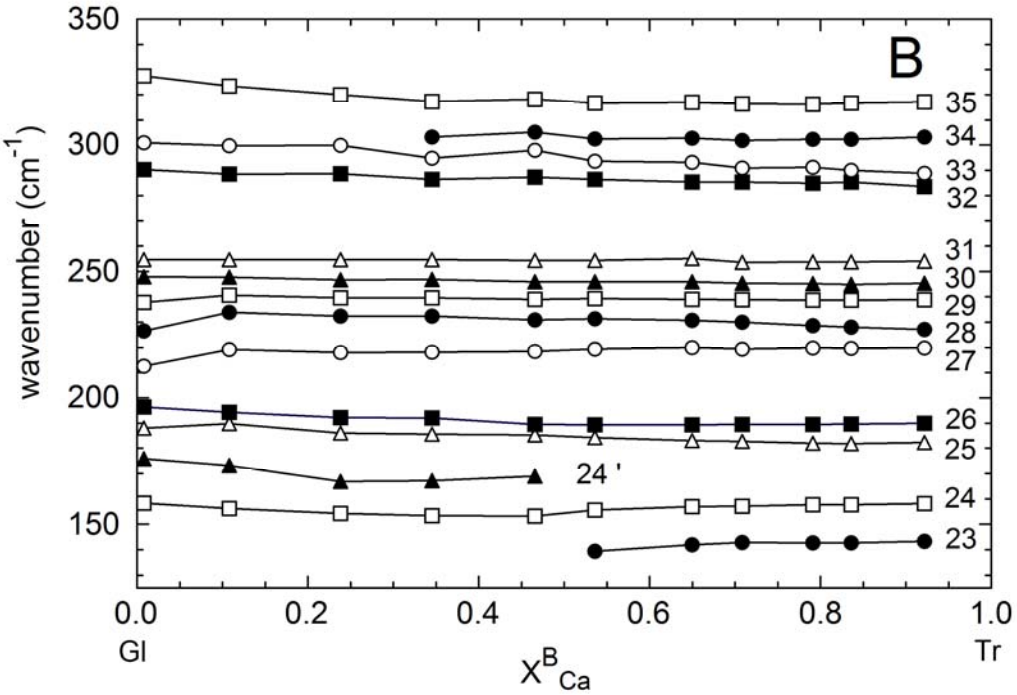

750
751

752 Figure 9

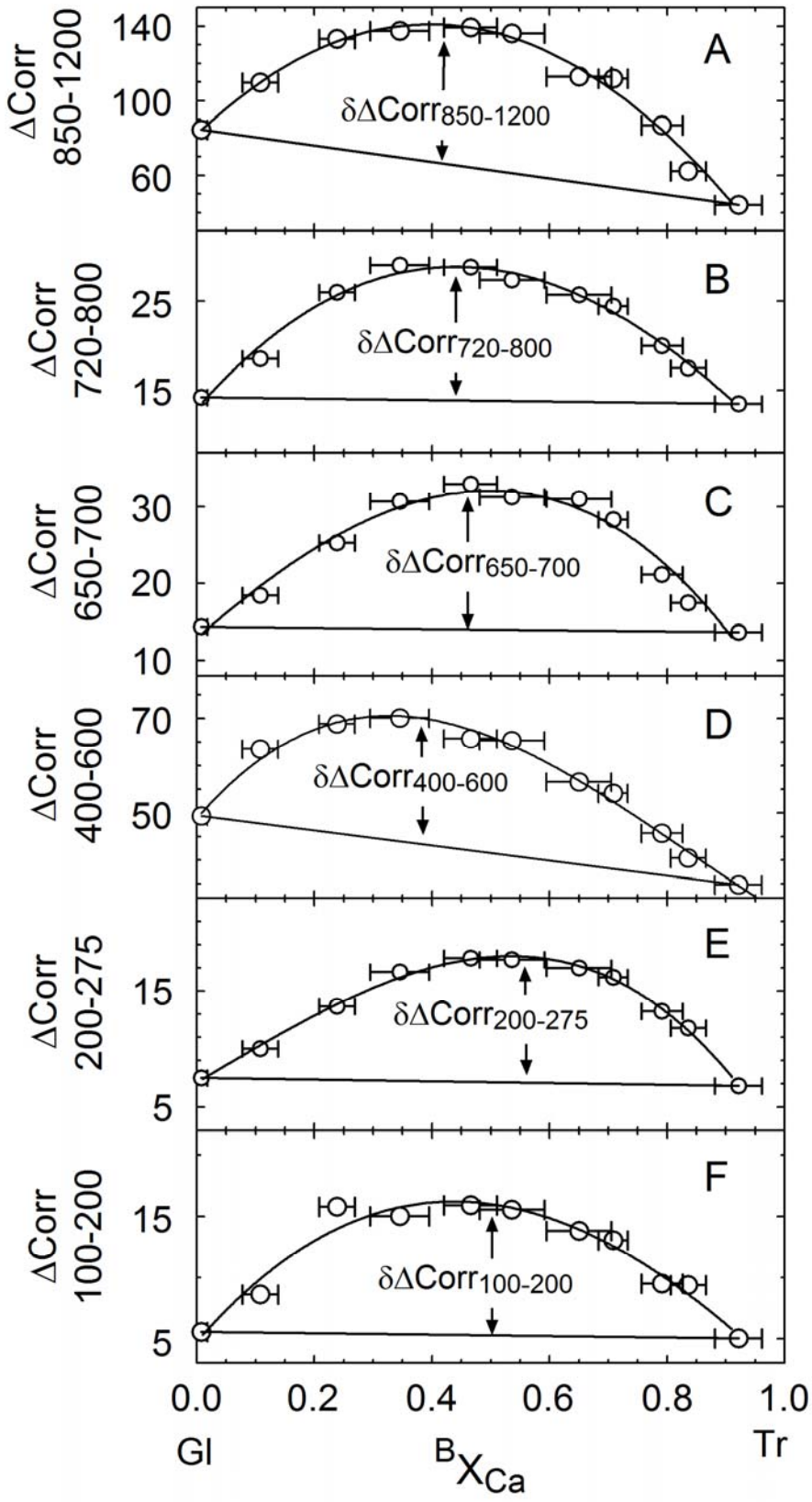

753
754

Figure 10

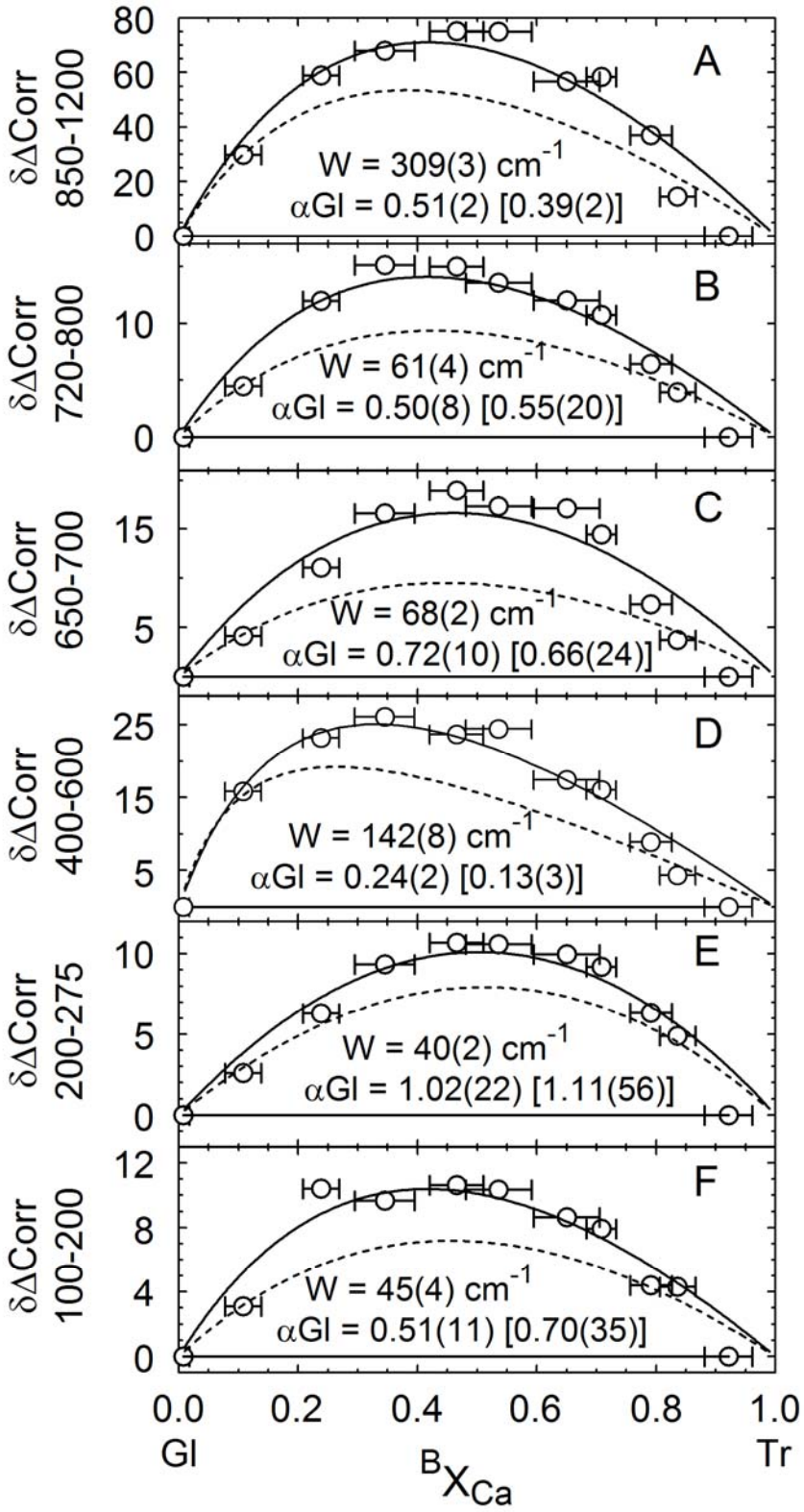

759 Figure 11
760

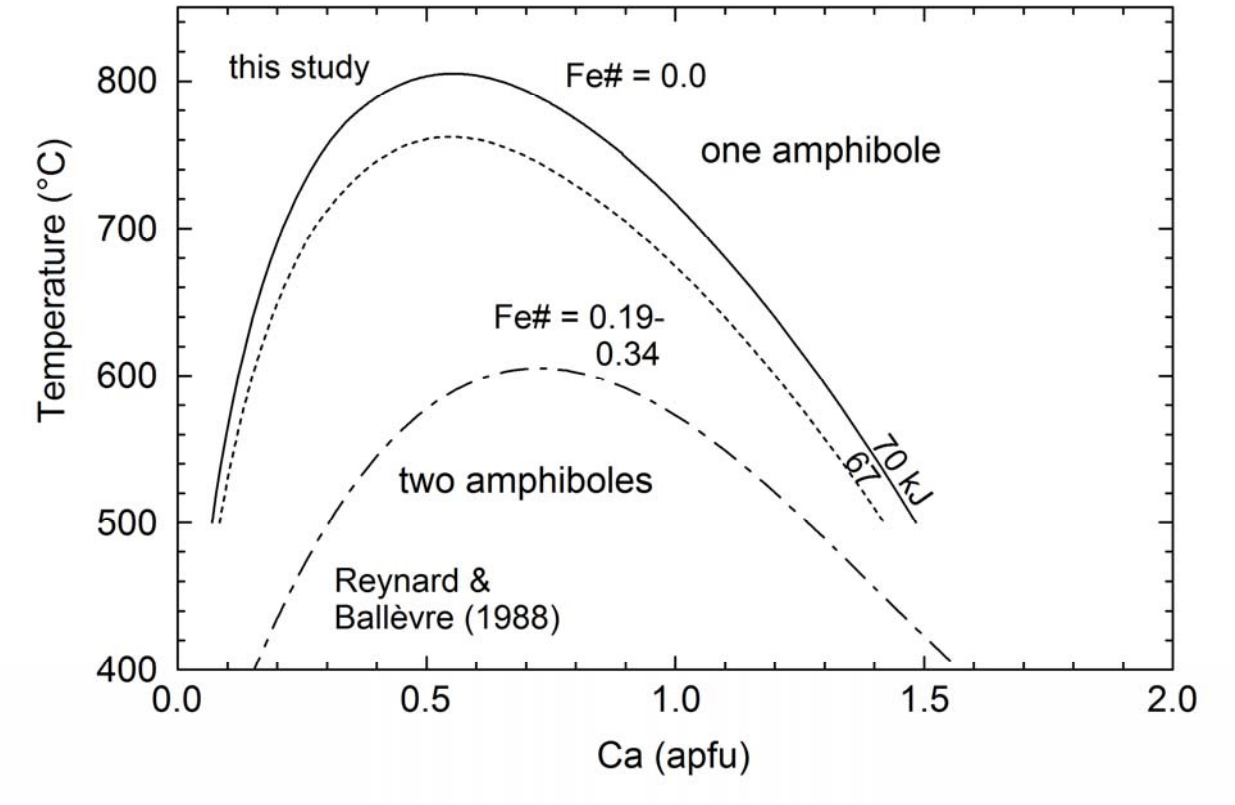

761